Adsorption of uranium (VI) complexes with polymer-based spherical activated carbon

Youssef-Amine Boussouga [1*], James Joseph [1], Hryhoriy Stryhanyuk [2], Hans H. Richnow [2], Andrea I. Schäfer [1]

[1] *Institute for Advanced Membrane Technology (IAMT), Karlsruhe Institute of Technology (KIT), Hermann-von-Helmholtz-Platz 1, 76344 Eggenstein-Leopoldshafen, Germany*

[2] *ProVIS-Centre for Chemical Microscopy, Department of Isotope Biogeochemistry, Helmholtz Center for Environmental Research (UFZ), Leipzig, Germany*

*Corresponding author: youssef-amine.boussouga@kit.edu (Y.-A. Boussouga), +49 721 608 24364

Revision submitted to

Water Research

10 October 2023

Abstract

Adsorption processes with carbon-based adsorbents have received substantial attention as a solution to remove uranium from drinking water. This study investigated uranium adsorption by a polymer-based spherical activated carbon (PBSAC) characterised by a uniformly smooth exterior and an extended surface of internal cavities accessible via mesopores. The static adsorption of uranium was investigated applying varying PBSAC properties and relevant solution chemistry. Spatial time-of-flight secondary ion mass spectrometry (ToF-SIMS) was employed to visualise the distribution of the different uranium species in the PBSAC. The isotherms and thermodynamics calculations revealed

monolayer adsorption capacities of 28 to 667 mg/g and physical adsorption energies of 13 to 21 kJ/mol. Increasing the surface oxygen content of the PBSAC to 10% enhanced the adsorption and reduced the equilibrium time to 2 hours, while the WHO drinking water guideline of 30 µgU/L could be achieved for an initial concentration of 250 µgU/L. Uranium adsorption with PBSAC was favourable at the pH 6-8. At this pH range, uranyl carbonate complexes ($UO_2CO_{3(aq)}$, $UO_2(CO_3)_2^{2-}$, $(UO_2)_2CO_3(OH)_3^-$) predominated in the solution, and the ToF-SIMS analysis revealed that the adsorption of these complexes occurred on the surface and inside the PBSAC due to intra-particle diffusion. For the uranyl cations (UO_2^{2+}, UO_2OH^+) at pH 2 to 4, only shallow adsorption in the outermost PBSAC layers was observed. The work demonstrated the effective removal of uranium from contaminated natural water (67 µgU/L) and meeting both German (10 µgU/L) and WHO guideline concentrations. These findings also open opportunities to consider PBSAC in hybrid treatment technologies for uranium removal, for instance, from high-level radioactive waste.

Keywords

Physico-chemical water treatment; carbonaceous activated carbon; uranyl; adsorption mechanisms; ToF-SIMS; adsorptive interactions

Graphical abstract

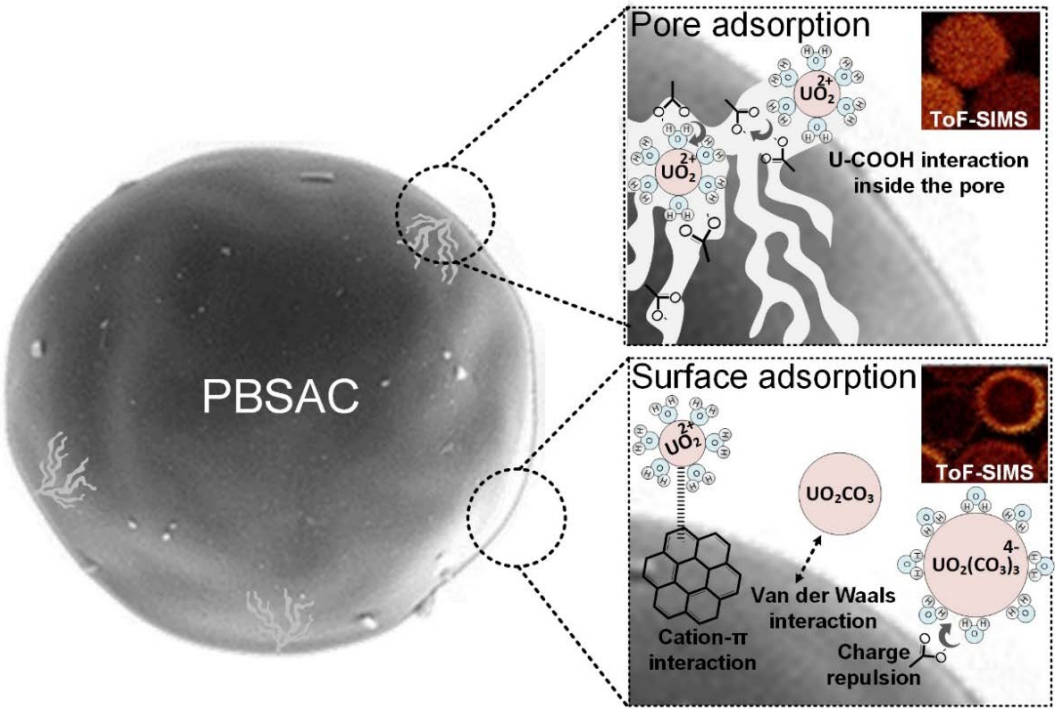

1. Introduction

The occurrence of uranium (U) in natural waters is a global threat to human health because of its chemitoxicity (Ansoborlo *et al.*, 2015; Lapworth *et al.*, 2021). Human health can be adversely affected by the poisoning of the lungs, liver, reproductive system, kidney, and bones (Ma *et al.*, 2020b). the World Health Organization (WHO) and the US Environmental Protection Agency (EPA) have set a uranium guideline of 30 µg/L in drinking water (EPA USA, 2018; WHO, 2017). Even stricter guideline values are suggested by Canada (20 µg/L) and Germany (10 µg/L) for drinking water (Banning and Benfer, 2017; Health-Canada, 2017). Uranium contamination in groundwater occurs either naturally through dissolution from mineral formations or through anthropogenic activities, such as mining, ore processing, and farming with a reported concentration in the range of < 0.1 µg/L to 69 mg/L across the world (Abd El-Magied *et al.*, 2021; Ma *et al.*, 2020b; Smedley and Kinniburgh, 2023; Waseem *et al.*, 2015). To meet the guidelines for typical global occurrence concentration (up to 69 mg/L), a treatment with ~100% U removal would be required.

Natural uranium is comprised of three radioactive isotopes: ^{238}U, ^{235}U, and ^{234}U. While ^{238}U is the most abundant with 99.28%, ^{235}U has an abundance of 0.72% and high radioactivity. The depleted

uranium (DU), on the other hand, which resulted from the enrichment process of ^{235}U, has 30% less radioactivity than natural uranium (Craft *et al.*, 2004). Depleted uranium is commonly used by the industry interested in the chemical and biological properties of uranium rather than its radioactive properties (Amrute *et al.*, 2013; Betti, 2003). Albeit the danger behind the exposure to radiation, the chemical toxicity of depleted or natural uranium is greater (Rump *et al.*, 2019).

Uranium in natural waters is principally found in the two stable oxidation states – U(VI) and U(IV). Under reducing conditions, U(IV) species of low solubility dominate, while in oxidizing environments, U(VI) predominates in the form of uranyl ion (UO_2^{2+}) (Alam and Cheng, 2014; Williamson *et al.*, 2014). The hydrated U(VI), or $UO_2(H_2O)_5{}^{2+}$, has a linear O=U=O entity with five water molecules that bind in a pentagonal fashion with a U-OH_2 distance of 2.48 Å (hydrated radius) (Aaberg *et al.*, 1983). This was recently supported by extended X-ray absorption fine structure (EXAFS) and quantum chemical calculations (Grenthe *et al.*, 2021). UO_2^{2+} cation is highly sensitive to hydrolysis (the loss of protons from bound water molecules) and can form stable complexes; particularly oxygen-containing ligands like OH^-, CO_3^-, SO_4^{2-}, PO_4^{4-} (Mühr-Ebert *et al.*, 2019; Nolan *et al.*, 2021; Smedley and Kinniburgh, 2023). The ternary complex $Ca_2UO_2(CO_3)_3$ is one extremely stable example (Endrizzi and Rao, 2014; Shang and Reiller, 2020). Uranium speciation and complexation are controlled by the physicochemical parameters including, pH, redox potential (Eh), and temperature (Catalano *et al.*, 2006; Götz *et al.*, 2011), as well as the presence of dissolved organic ligands (Bone *et al.*, 2020). For the distribution of U(VI) species in a ternary $UO_2^{2+}/CO_3^{2-}/H_2O$ open system, such as in the case of an oxidizing freshwater, UO_2^{2+} and its hydrolysed forms $UO_2(OH)^+$ and $UO_2(OH)_2$ are predominant up to pH 6, whereas from pH 7, the carbonate complexes, such as $UO_2CO_{3(aq)}$, $UO_2(CO_3)_2^{2-}$ and $UO_2(CO_3)_3^{4-}$ are formed (Krestou and Panias, 2004). When including SO_4^{2-}, PO_4^{4-}, SiO_4^{2-} and F^-, further complexes UO_2SO_4, UO_2HPO_4, $UO_2(OH)_3SiO_4^+$ and UO_2F^+ can be formed at pH $\leq$ 6, and ternary uranyl carbonates complexes are formed in the presence of Mg and Ca at pH $\geq$ 7 (Smedley and Kinniburgh, 2023). The characteristics of uranyl and uranyl carbonate species $UO_2^{2+}/CO_3^{2-}/H_2O$ in an open system are reported in Table 1.

Table 1. Characteristics of uranyl species in the ternary $UO_2^{2+}/CO_3^{2-}/H_2O$ system

U(VI) species	Hydration radius [a] (Å)	Hydration number [a]	Gibbs free energy of formation [b] (kJ/mol)	Diffusion coefficient [b] ($10^{-10}m^2/s$)
UO_2^{2+}	2.48 (U-O_{H_2O})	5	–952	7.6
UO_2OH^+	-	-	–1160	-
$UO_2(OH)_{2\ (aq)}$	-	-	–1368	-
$UO_2CO_{3\ (aq)}$	2.34 (U-$O_{CO_3^{2-}}$)	3	–1536	6.7
$UO_2(CO_3)_2^{2-}$	2.4 (U-$O_{CO_3^{2-}}$)	1	–2105	5.5
$UO_2(CO_3)_3^{4-}$	2.39 (U-$O_{CO_3^{2-}}$)	0	–2660	5.6

[a] *The values of the hydration radius and hydration number of the different uranium species are taken from Kerisit and Liu (2010).*
[b] *The Gibbs free energy and diffusion coefficient values are from Grenthe et al. (1992).*

Common technologies used for uranium removal from water are classified into chemical methods, such as precipitation (Mellah *et al.*, 2007), bioremediation by (bio)sorption (Krawczyk-Bärsch *et al.*, 2018), and physiochemical methods, such as nanofiltration/reverse osmosis (NF/RO) (Shen and Schäfer, 2014) and adsorption (Tian *et al.*, 2021). NF/RO membranes can achieve 90-99% of uranium removal (EPA, 2007). However, uranium can be adsorbed and saturated in the membrane material (Schulte-Herbrüggen *et al.*, 2016; Torkabad *et al.*, 2017), for example by the attachment of the positive U(VI) complexes to the negative COO^- entities of polyamide (PA) (Torkabad *et al.*, 2017), which is the most common material used in NF/RO fabrication (Karan *et al.*, 2015).

Adsorption, on the other hand, is widely used for uranium removal, because it is generally more practical, easily scalable, and efficient compared to other methods, with a large number of inorganic-based adsorbents (Bakhsh *et al.*, 2022; Calì *et al.*, 2018; Fan *et al.*, 2012; Thapa *et al.*, 2021; Zhao *et al.*, 2023a), organic (carbon) based adsorbents (Donat and Erden, 2017; Hu et al., 2016; Yi et al., 2020b; Zhao et al., 2017), framework materials (Guo et al., 2021; Jun et al., 2021), and composite nanomaterials (Abd El-Magied *et al.*, 2021; Song *et al.*, 2021; Zhu *et al.*, 2021a). Carbon-based adsorbents and composite nanomaterials can offer a higher adsorption capacity than inorganic and framework materials, which in addition, exhibit inferior mechanical properties and are difficult to recycle (Jun et al., 2021; Ma et al., 2020a). Carbon materials, for instance, are characterised by large

specific surface areas, pore volumes, high heat resistance, and ease of functionalisation (Jun *et al.*, 2021), and thus are widely used for uranium removal (Table S1).

Granular activated carbon (GAC) and powdered activated carbon (PAC) are the most common adsorbents in water treatment (Worch, 2021) and have been applied for uranium removal (Caccin *et al.*, 2013; El-Sayed, 2008; Mellah *et al.*, 2006). Such conventional activated carbon materials (GAC and PAC) are formed by the carbonisation and activation of natural carbon sources, such as coconut shells, coal, or pitch (John Presin Kumar *et al.*, 2021). This generally results in a non-uniform shape, internal surface area, and wide pore size distribution which affect the adsorption properties (Müller, 2010). To achieve a more well-defined carbon-based material with a narrower pore size distribution, a polymeric precursor strategy can be employed (Chen *et al.*, 2018; Huang *et al.*, 2021). This is the case of polymer-based spherical activated carbon (PBSAC) which is produced in a batch process by carbonisation of the non-porous starting material followed by activation to establish the pore system as described elsewhere (Böhringer *et al.*, 2011).

PBSAC has a higher specific area (1769 to 2125 m^2/g) and pore volume (0.65 to 1.29 cm^3/g) compared to conventional PAC (505 to 1676 m^2/g, 0.35 to 0.89 cm^3/g (Partlan *et al.*, 2016)). In addition, the pore size of PBSAC (1.3 to 2.3 nm (Tagliavini *et al.*, 2017)) is larger than the ionic (0.1 to 0.2 nm (Bastrakov *et al.*, 2010)) and hydrated (0.5 to 0.9 nm) (Nichols *et al.*, 2008) diameter of uranyl species. This could result in fast adsorption kinetic and enhanced internal transport. Schrage *et al.* (2014) have previously investigated unmodified (<1 % surface oxygen content) and modified PBSAC (15% surface oxygen content) with a reported uptake at pH 5 of 0.3 mg/g and 8 mg/g, respectively. The results were explained by the electrostatic interaction with the carboxyl groups of the oxidised carbon on the surface. However, the kinetics and the isotherms as well as the potential adsorption and mass transfer mechanisms at different uranium species are unknown.

In carbon-based materials, uranium adsorption occurs generally through physical adsorption, mainly through electrostatic attraction by specific functional groups, such as coordination/complexation by donor ligands, and ion exchange processes (Jun *et al.*, 2021). Weaker intermolecular van der Waals

interactions, hydrogen bonding, cation/π, and hydrophobic interactions can also contribute to uranium adsorption (Duan *et al.*, 2021; Wang *et al.*, 2022b). Recent varieties of AC highlight their functionalised surface and large pore volume as the primary reason for uranium adsorption, while the interaction with the functional moieties, (especially O-containing) such as C=O, OH, COOH, C=O facilitate physical adsorption (Alahabadi *et al.*, 2020; Aslani and Amik, 2021; Kütahyalı and Eral, 2004; 2010; Zhu *et al.*, 2021b).

The interactions between uranium and AC are dependent on uranium speciation and AC surface chemistry at different pH. Due to the various functional groups on their surfaces and the presence of a π electron system that confers them with Lewis basic properties, AC materials are amphoteric by nature and generally exhibit a positive charge pH < 5 (Chingombe *et al.*, 2005; Julien *et al.*, 1998). This hinders the adsorption as uranium species at pH < 5 (UO_2^{2+}, UO_2OH^+) are positively charged (Mellah *et al.*, 2006; Wang *et al.*, 2022b). The pH range 5.0 to 6.5 has been reported as the best adsorption window due to the electrostatic interaction between positive uranyl (UO_2^{2+}, UO_2OH^+) species and the deprotonated functional groups (–OH, –COOH) of the AC at this pH (Abd El-Magied *et al.*, 2021; Alahabadi *et al.*, 2020; Aslani and Amik, 2021; Belgacem *et al.*, 2014; Guo *et al.*, 2021; Kütahyalı and Eral, 2004; Mellah *et al.*, 2006; Song *et al.*, 2021; Villalobos-Rodríguez *et al.*, 2012; Yaman and Demirel, 2021; Yi *et al.*, 2020b; Zhang *et al.*, 2021b; Zhu *et al.*, 2021b). At pH >7, most of the reported AC surface becomes negative due to the deprotonation of functional groups and anionic uranyl complexes ($UO_2(CO_3)_2^{2-}$, $UO_2(CO_3)_3^{4-}$) are subsequently repelled from the AC surface (Abd El-Magied *et al.*, 2021). While conventional AC achieves limited adsorption capacity due to the non-selective adsorption sites, functionalised carbon-based adsorbents with specific functional groups having high affinity to uranium can be more selective and thus exhibit higher adsorption capacities (Table S1). A recent study demonstrated that carbon-based adsorbents with grafted phosphoric acid groups could achieve an adsorption capacity of 617 mgU/g (at pH 4.5) and 3 s to achieve equilibrium (Zhao *et al.*, 2023b). This is simply because of the high chelating affinity of uranyl ions/complexes to phosphate groups (Yang *et al.*, 2015). However, the complex preparation

processes such functionalised carbon-based adsorbents always need highly toxic, flammable, and volatile chemicals, which can lead to secondary pollution, hence hindering their scale-up (Wang *et al.*, 2022a). PBSAC, on the contrary, is developed with a simple process from a well-defined precursor and exhibits a very smooth and uncharged carbonaceous surface with high pore volume and surface area (Böhringer *et al.*, 2011), while the adsorption mechanisms have not been identified for uranium species. Due to the carbonaceous surface, the relevant mechanism is likely to be physical adsorption originating from weaker short-range interactions between uranium and the carbon surface (Guo *et al.*, 2021; Xie *et al.*, 2019).

Universal short-ranged van der Waals interactions of low binding strength are expected to be relevant in facilitating physical adsorption (Israelachvili, 2011; Petrovic *et al.*, 2022; Pourhakkak *et al.*, 2021), as reported for various heavy metals, including uranium (Srivastava *et al.*, 2021). Cation-π interaction (a short-range force <0.5 nm) with the polarised π-electron rich region was reported to be an important interaction for heavy metals (Mahadevi and Sastry, 2013; Shi *et al.*, 2013; Tran *et al.*, 2017a; Yi *et al.*, 2020a; Zhang *et al.*, 2021a). This mechanism applied to uranium removal using AC fibre-titanate nanotubes composite (Duan *et al.*, 2021), modified graphene oxide (Amini *et al.*, 2021), biochars (Hu *et al.*, 2018; Xu *et al.*, 2020) and pine-derived carbon (Philippou *et al.*, 2018) showing the affinity of uranium towards surfaces rich in π electrons. Following the adsorption of the adsorbate to the surface of the adsorbent, surface diffusion and intra-particle diffusion occur to enter the pores (Sahoo and Prelot, 2020). The presence of carboxylic groups inside the pores can exert an attractive force on the surface-adsorbed uranium, which facilitates the diffusion of uranium into the pores of PBSAC (Schrage *et al.*, 2014). In order to visualise uranium species adsorbed and elucidate possible mechanisms, time of flight secondary ion mass spectrometry (ToF-SIMS), which performs chemical imaging of surfaces and depth profiling with high mass and spatial resolution, can be employed (Han *et al.*, 2020; Proriol Serre *et al.*, 2019; Zhao *et al.*, 2020). ToF-SIMS can offer more sensitive analysis with greater chemical selectivity than other surface and interface analysis techniques, such as X-ray photoelectron spectroscopy (XPS), with 1 to 2 nm information depth (Watts and Goacher, 2022).

Such a method (ToF-SIMS) has previously investigated uranium adsorption in organic materials (Yang *et al.*, 2022).

While the adsorption of uranium was previously investigated with PBSAC (Schrage *et al.*, 2014), fundamental mechanisms that underpin this adsorption were investigated in this study. Uranium removal with PBSAC was confirmed with contaminated natural water. The specific research questions are: i) what are the adsorption kinetics, isotherms, and thermodynamics of uranium with PBSAC?; ii) what are the dominating adsorption mechanisms (short- and long-range interactions) of the different uranium species with PBSAC?; and iii) what is the limiting mass transfer step (surface adsorption, intra-particle diffusion) during the adsorption process of uranium with PBSAC?

2. Materials and methods

2.1. Polymer-based spherical activated carbon material

PBSAC of different sizes and surface oxygen content were provided by Blücher GmbH (Erkrath, Germany). Material characteristics of PBSAC, including particle diameter, surface oxygen content, activation level, tap density, and surface area are summarised in Table 2. Morphology imaging and surface chemistry characterisation can be found elsewhere (Tagliavini *et al.*, 2017; Trinh and Schäfer, 2023), in which the results confirmed the homogenous size, spherical shape, and micropores distribution, with a hydrophobic character and uncharged surface over the pH range 4.5–9.5.

Table 2. Proprieties of the various PBSAC investigated in this work (Böhringer *et al.*, 2011; Tagliavini *et al.*, 2017)

PBSAC Code	Average particle diameter (µm)	Surface oxygen content (%)	Activation level	Tap density (g/mL)	Surface Area (m^2/g)
MKD 200	200	5	4	0.60	1440
MKD 450	450	5	4	0.40	1920
O1.5	200	1.5	4	0.60	1436
O10	200	10	4	0.59	1436

2.2. Static adsorption experiments

To evaluate the kinetics, isotherms and thermodynamics of uranium adsorption to PBSAC, static adsorption tests were conducted using an incubator shaker (Innova 43 R, New Brunswick Scientific, USA). Varying amounts of PBSAC according to the desired concentrations (0.01-10 g/L) were measured using an analytical balance (AC 210P, Sartorius, Germany) and transferred (without any pre-treatment) into conical shaker flasks (250 mL, Duran group, Germany) containing 250 mL uranium solution. Once the PBSAC was added to the adsorbate solutions, the shaker was set to a constant temperature of 20°C and a shaking speed of 260 rpm for 26h. For adsorption thermodynamics, the temperature was varied from 10 to 80 °C. 5 mL of samples of supernatant (PBSAC-free) were extracted using a 5 mL pipette (Eppendorf, Germany) at a defined interval (7, 10, 15, 30, 45, 60 min, and 2, 3, 5, 7, 9, 24, 26 h). The samples were stored in 5 mL plastic vials, acidified at 2% (w/w) HNO_3 (Merck, Suprapure 65%, Germany) and kept at an ambient temperature until ICP-MS analysis.

2.3. Uranium and solution chemistry

A stock solution of 1 g/L U was made by diluting 16.7 mg of uranyl chloride hydrated ($UO_2Cl_2.3H_2O$) (IBILABS, purity 99.9%, USA) in 100 mL Milli-Q water (MilliQ A+ system, Millipore, Germany). The stock solution was used to prepare the adsorbate solutions of different uranium concentrations (0.25 to 100 mgU/L) in a background comprised of 1 mM $NaHCO_3$ (Bernd Kraft, purity ≥99.7%, Germany) and 10 mM (0.58 g/L) NaCl (VWR chemicals, purity ≥99.9%, Germany). The required $NaHCO_3$ and NaCl volumes were added from 100 mM $NaHCO_3$ (8.4 g/L $NaHCO_3$, pH 8.3±0.1) and 1 M NaCl (58.4 g/L NaCl, pH 6.5±0.1) stock solutions prepared in MilliQ water. The pH was adjusted using 1 M HCl prepared from HCl 37% solution (Roth, Germany) and 1 M NaOH prepared from dissolved NaOH pellets (Merck, purity ≥99%, Germany).

2.4. Menzenschwand spring water

Natural water samples containing uranium were collected from various sites close to Krunkelbach Pit near the municipality Menzenschwand (Waldshut, Baden-Württemberg, Germany) on 02/06/2021,

where a spring water conduit which contained significant levels of uranium (N47°50.332‘E008°02.824; Figure S1) was selected for investigating uranium adsorption with PBSAC in real water conditions. The water characteristics of the different collected samples are detailed in Table S2. Krunkelbach Pit was known for investigating and exploiting uranium deposits from 1961 until 1991 in the Menzenschwand region. The mining operation was shut down due to various protests (Steen, 2004). Since 2005, water from the uranium ore deposit has been used to run a radon bath in Menzenschwand, and the natural occurrence provided a suitable ‘real water’ for verification of results.

2.5. Water analysis

Uranium analysis was performed with inductively coupled plasma - mass spectrometry (ICP-MS) (Agilent, model J8403A 7900 ICP-MS, Japan). For calibration, standard solutions with 0.25 – 1000 µgU/L were prepared from uranium stock solutions of 0.5 and 2 mgU/L acidified in 2% (w/w) HNO_3 (Merck, Suprapure 65%, Germany). The concentration of uranium in the stock solutions was verified with ICP multi-element standard (ICP standard solution VI 30 elements, 9.9 ± 0.5 mgU/L, Certipur®, Germany). Calibrations and limit of detection (LOD) are shown in Figure S2.

For water analysis of the real water sample, ion chromatography (IC) (Metrohm 580 Professional, Switzerland) with an anion exchange column (A Supp 5 column, Metrohm, Switzerland) was used to determine anion concentrations (see calibration curve and LOD in Figure S3). For total organic carbon (TOC) and inorganic carbon, a total carbon analyser (TOC-LCPH FA E200, Shimadzu, Japan) was used (see calibration curves and LOD in Figure S4).

The pH and electrical conductivity (EC) were measured using a multi-parameter portable meter (WTW ProfiLine pH/Con 3320, Germany) with separate pH (WTW SenTix 81, Germany) and conductivity (WTW TetraCon 325, Germany) sensors. pH sensors were calibrated using technical buffer solutions of pH 4, 7, and 10 (WTW, Germany). The EC sensor was calibrated using a calibration standard of 0.01 M KCl (WTW, Germany).

2.6. Adsorption kinetics and isotherms models

In aqueous-phase adsorption, various kinetic reaction models can be used to mathematically describe the intrinsic kinetic adsorption constant, and therefore, establish the required contact time for effective adsorption. The pseudo-first-order (Eq. (1) (Lagergren, 1898)), pseudo-second-order (Eq. (2) (Blanchard *et al.*, 1984)), and intraparticle diffusion (Eq. (3) (McKay *et al.*, 1980)) models are commonly applied for this purpose.

$$q(t) = q_e(1 - e^{-kt}) \tag{1}$$

$$q(t) = \frac{q_e^2 k_2 t}{1 + k_2 q_e t} \tag{2}$$

$$q(t) = k_d t^{0.5} + \text{const} \tag{3}$$

where q(t) (µg/g) is the uptake of the adsorbate, uranium in this case, as a function of time t (h), q_e (µg/g) is the uptake at equilibrium, k (1/h), k_2 (g/µg·h), k_d (µg/g·$h^{0.5}$) are kinetic rate constants, and const (µg/g) is the constant parameter of the intraparticle diffusion model, that depends on the thickness of the boundary layer (Wang *et al.*, 2022c).

The kinetic rate constants of pseudo-first-order and pseudo-second-order can indicate the speed of the adsorption, depending upon the concentration of the adsorbate (Bhalara *et al.*, 2014; Saha and Grappe, 2017). However, pseudo-second-order can fit better if the quantity of accessible adsorption sites is assumed to be in excess, while pseudo-first-order is expected to fit better at low quantities of adsorption sites (Guo and Wang, 2019; Liu and Shen, 2008). It should be noted that these models are empirical and do not indicate explicitly which adsorption mechanism (film diffusion or intraparticle diffusion) is limiting. The kinetic rate constant k_d indicates the speed of adsorbate diffusion into the pores of the adsorbent, and this process is generally slow and can be controlled by multiple processes (film diffusion, surface adsorption, and surface diffusion) (Wang and Guo, 2022). For this, the pores of the PBSAC are assumed to be big enough to allow uranium diffusion, and this is true since the

hydrated diameter of uranyl species (0.5-0.9 nm (Nichols *et al.*, 2008)) is smaller than the pore size of PBSAC (1.3-2.3 nm (Tagliavini *et al.*, 2017)).

Adsorption isotherms, on the other hand, are used to fundamentally understand the interaction of the adsorbate with the adsorbent, while describing the adsorption behaviour, as well as the adsorption efficiency and capacity at specific conditions (Al-Ghouti and Da'ana, 2020). Various adsorption isotherm models have been used in the literature. The Freundlich and Langmuir models are the most commonly used due to their simplicity, the significance of their model parameters and their easy interpretability (Tran *et al.*, 2017b). While the Freundlich isotherm is an empirical model (Eq. (2) (Freundlich, 1907)) used for multilayer adsorption on heterogeneous sites, the Langmuir isotherm is a model based on kinetics principles (Eq. (5) (Langmuir, 1918)) and assumes a monolayer reversible adsorption with a fixed number of adsorption sites. In contrast to Langmuir, Freundlich isotherm does not describe the saturation behaviour of an adsorbent, where the PBSAC surface area is in excess compared to uranium (Table S3 and Table S4).

$$q_e = K_F c_e^{1/n_f} \tag{4}$$

$$q_e = \frac{q_m K_L c_e}{1 + K_L c_e} \tag{5}$$

where c_e is the equilibrium concentration of uranium (mg/L), K_F is the Freundlich constant (mg/g), n_F is the heterogeneity factor (unitless), q_m is the maximum adsorption capacity (mg/g) and K_L is the Langmuir constant related to the energy or enthalpy of adsorption (L/mg).

2.7. Thermodynamic parameters and adsorption energy

Thermodynamic parameters comprising of Gibbs free energy change (ΔG^0), enthalpy change (ΔH^0), and entropy change (ΔS^0) are used to identify whether the prevailing adsorption mechanism is physical or chemical (Tran *et al.*, 2016). ΔG^0 is calculated using Eq.(6) and Eq. (7), while ΔH^0 and

ΔS^0 are calculated as the slope and intersect of the plot between the equilibrium adsorption coefficient (K_d, dimensionless) and 1/T (Eq. (8)):

$$\Delta G^0 = -R_g T \ln K_d \tag{6}$$

$$K_d = \frac{q_e \cdot m_{PBSAC}}{c_e \cdot V} \tag{7}$$

$$\ln K_d = \frac{\Delta S^0}{R_g} - \frac{\Delta H^o}{R_g T} \tag{8}$$

where R_g is the ideal gas constant (8.314 J/mol.K)

If uranium adsorption to PBSAC was predominantly physical adsorption due to electrostatic interactions (Schrage *et al.*, 2014), then a negative value with a high magnitude of ΔG^0 would suggest that these interactions are energetically favourable (Haynes, 2016; Tran *et al.*, 2016). In such a case, ΔH^0 would be negative as well (Tran *et al.*, 2016), and the magnitude of ΔH^0 would indicate the interaction strength between uranium and the PBSAC surface. Exothermic adsorption with a lower strength of uranium binding (as exhibited by interactions such as H-bonding and cation-π) would be reflected with a magnitude of $\Delta H^0 < 40$ kJ/mol (Inglezakis and Zorpas, 2012).

In physical adsorption, the activation energy (E_a, J/mol) is below the E_a range of chemical adsorption (40 to 800 kJ/mol) and a lower magnitude would indicate weak binding (Tran *et al.*, 2016). E_a is determined from the kinetic rate constant (k) using Eq. (9):

$$\ln k = -\frac{E_a}{R_g T} + \ln A \tag{9}$$

where A (1/h) is the Arrhenius constant.

2.8. Data Analysis

Removal (R, %) of uranium by PBSAC at a specific time from the start of static adsorption is calculated using Eq. (10), while the adsorption uptake q(t) (µg/g) at a specific time is calculated using Eq. (11):

$$R = \frac{c_0 - c(t)}{c_0} \cdot 100 \tag{10}$$

$$q(t) = \frac{c_0 - c(t)}{m} \cdot V \tag{11}$$

where c_0 (µg/L) is the initial uranium concentration and c(t) (µg/L) is the concentration of uranium at time t (h), m (g) is the mass of PBSAC and V (L) is the volume of the supernatant.

The error associated with R(t) and q(t) were estimated through experimental error propagation (Figure S5).

2.9. Time of flight – secondary ion mass spectrometry analysis

The PBSAC samples used for uranium adsorption were analysed, with a focus on the ^{238}U isotope, using TOF-SIMS 5 instrument (IONTOF GmbH, Münster, Germany) operated in both imaging and spectrometric modes. In both operation modes, 30 keV Bi_3^+ cluster ions from the liquid metal ion gun (LMIG) NanoProbe source were employed as primary probe-projectiles in a double-beam approach, involving an electron-impact source of 1 keV O_2^+ (300 nA) for sample sputtering in non-interlaced may. The charge compensation was carried out in two ways: (i) 21 eV electrons flooding the surface of the analysed sample after each shot with the primary Bi_3^+ beam and (ii) Ar gas injection system (Ar-GIS) maintaining the partial Ar gas pressure at $4 \cdot 10^{-6}$ mbar ($4 \cdot 10^{-4}$ Pa) in the analysis chamber.

Imaging mode was done in delayed extraction (analysis duration 26 h) to achieve a mass resolving power (MRP) of over 5000 and a lateral resolution of about 100 nm. This high-resolution "delayed-extraction" mode (Benettoni *et al.*, 2019) was employed for the initial localisation and identification of uranium-containing phases in the PBSAC samples. The high lateral resolution of the imaging mode

was achieved at the cost of the primary Bi_3^+ ion beam current reaching 0.02 pA with a 100 µs repetition period. Analysis in this mode was performed by rastering the primary ion beams randomly in 2048×2048 pixels over a 300×300 µm² field of view.

Spectrometry operation mode (analysis duration 14 to 24 h) possessing high mass-resolving power and higher current of primary Bi_3^+ ions (0.5 pA with 100 µs repetition period) was employed with a lateral resolution of 5 µm. The 35 ns Bi_3^+ ion bunch was compressed (bunched) to probe samples with high mass-resolving power (MRP above 7000) over a 500×500 µm² area in randomly located 512×512 pixels. Data evaluation was performed using SurfaceLab 7.1 software (ION-TOF GmbH). Having the highest count rate, the mass peak at 270.04 m/z, corresponding to secondary UO_2^+ ions, was employed to identify uranium species for uranium analysis in the spectrometry mode of ToF-SIMS operation. The detailed mass spectrum of UO_2^+ and UO_2^+–R fragments (down to $^{237}U^+$) is shown in Figure S7, while the ToF-SIMS images of PBSAC in delayed extraction mode showing both UO_2^+ and UO_2^+-R fragments upon sputtering with 1 keV O_2^+ ion beam are shown in Figure S8.

For sample preparation, and in order to inhibit further uranium diffusion inside the pores, the PBSAC samples were frozen and then lyophilised at –15 °C in a freeze dryer (Alpha LSC plus, Martin Christ Germany) for approximately 30 hours until all moisture had been sublimated. Before ToF-SIMS analysis, the freeze-dried PBSAC samples were exposed to a vacuum of 10^{-1} mbar (10 Pa) for 30 minutes and flooded with Ar gas in 3 cycles. PBSAC samples were then immersed into 100% LR-white resin (London Resin medium, soft uncatalysed, Agar Scientific, UK) medium in 2 mL tubes and were kept at 80 mbar pressure for 1 hour to facilitate the resin infiltration. The resin was used to keep the PBSAC together and fixed mechanically upon trimming. The tube with resin-immersed PBSAC was then shaken for 24 hours using PTR-35 Multi-Rotator (Grant Instruments, Cambridge UK) reciprocally within ±60° angle at 3 rpm speed and vibrating within ± 5° for 5 s in each extreme (when tubes were slanted at +60° and –60° relatively to vertical orientation). Tubes with infiltrated samples were kept without motion at room temperature for the next 24 hours to let PBSAC settle well. Resin polymerisation was performed at 60°C for 48 hours, followed by cross-sectioning of resin-

embedded samples using a Leica EM TRIM2 trimmer equipped with a diamond cutter to get a flat section for ToF-SIMS analysis. To fit samples of resin-embedded PBSAC into a holder frame (7.8 mm diameter) made of polyetheretherketon (PEEK), the prepared cross-section was levelled and the sample height was adjusted. The insulating sample frame was employed to reduce the distortion of the equipotential surface under the analyser extractor and focusing lenses of ion/electron sources with the charging sample. Figure S6 illustrates the different stages of the PBSAC preparation for TOF-SIMS analysis.

3. Results and discussion

Static adoption of uranium with PBSAC was investigated for varying adsorbent characteristics (surface area, surface oxygen content) and relevant solution chemistry (uranium concentration, pH). The kinetics, isotherms and thermodynamics were analysed to elucidate the adsorption mechanisms, while adsorption was visualised by ToF-SIMS analysis. The first parameter investigated was the exposure time to establish the adsorption equilibrium time.

3.1. Equilibrium time of uranium adsorption with PBSAC

To quantify the equilibrium time of uranium adsorption by PBSAC, static adsorption experiments were performed with MKD 200 and MKD 450 at a dose of 1g/L, and an environmentally relevant uranium concentration of 250 µgU/L (Smedley and Kinniburgh, 2023) (Figure 1A, B, C). ToF-SIMS analysis was used to visualise the adsorption (Figure 1D). The pixel-resolved uranium content in PBSAC samples is shown in Figure S9.

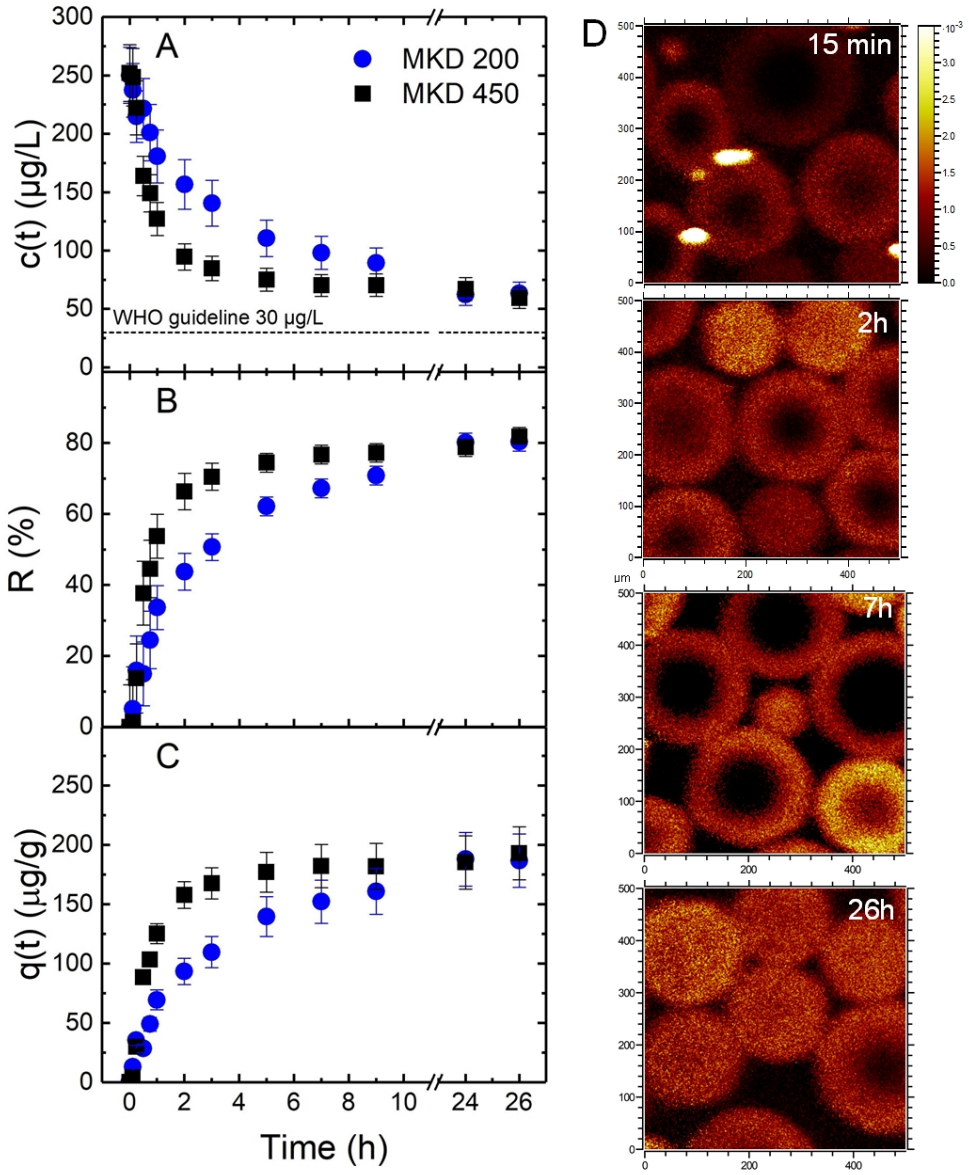

Figure 1. (A) uranium concentration, (B) removal and (C) uranium uptake as a function of time using 1 g/L PBSAC (MKD 200 and MKD 450). (D) ToF-SIMS images of PBSAC MKD 200 in spectroscopy mode showing the progression of adsorption of UO_2^+ at varying exposure times (c_0 250 µgU/L, 1 mM $NaHCO_3$, 10 mM NaCl, 20°C, 260 rpm, pH 8.1±0.3).

Both types of PBSAC (MKD 200 and MKD 450) removed uranium from water. Uranium concentration dropped from 250 to 60 µg/L, corresponding to a removal of about 80%, while the WHO guideline was not reached (Figure 1A). Prior equilibrium, MKD 450 exhibited higher uptake than MKD 200, which can be attributed to the higher pore volume of MKD 450 (1.3 cm^3/g compared to MKD 200 0.65 cc/g (Böhringer *et al.*, 2011)). The equilibrium uptake of 185 ± 20 µg/g was reached at 7 hours for MKD 450, while MKD 200 required 24 hours to attain equilibrium (Figure 1C).

ToF-SIMS analysis revealed that the adsorbed uranium was detected both on the surface and inside the PBSAC, while the centre of the PBSAC remained unoccupied at 15 minutes, 2 hours, and 7 hours, (Figure 1D). The internal part of most PBSAC appears to be completely occupied after 26 hours at pH 8.1±0.3 (Figure 1D). This indicates that the adsorption of uranium on the PBSAC surface was followed by the intra-particle diffusion in the pores of the PBSAC. The latter mechanism is significant for adsorbents with high porosity (Pauletto *et al.*, 2020), such as the case of PBSAC, in which 98% of the surface area consists of micro and mesopores with a diameter of less than 5 nm (Tagliavini *et al.*, 2017).

In the next section, apparent adsorption kinetics will be determined as a function of PBSAC dose and type.

3.2. Kinetics of uranium adsorption with different PBSAC dosages

Apparent adsorption kinetics with different PBSAC types, uranium equilibrium concentration (c_e) with the respective removal, uranium uptake at equilibrium (q_e) and kinetic rate constant (k) with increasing PBSAC dose were investigated (Figure 2). When surface area is the limiting factor, an increase in the PBSAC dosage will enhance the removal, knowing that the surface area of the PBSAC was always in excess (Table S4). Concentration, uptake, and removal of uranium as a function of time and pseudo-first order fitting parameters can be found in Figure S11 and Table S5. Experimental data fittings with pseudo-second-order and intraparticle diffusion models are shown in Figure S12, Figure S13, and Table S6.

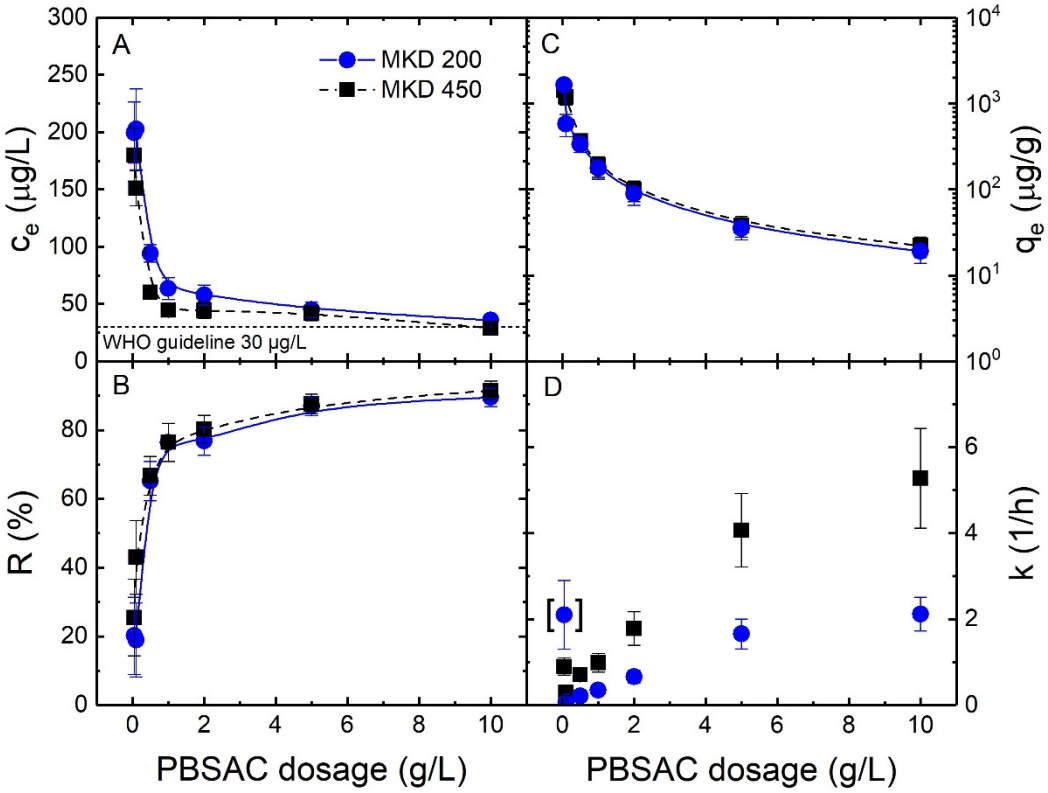

Figure 2. (A) uranium equilibrium concentration, (B) removal, (C) uranium uptake at equilibrium with their respective (D) k at different PBSAC dosages for MKD 200 and MKD 450 (c_0 250 µgU/L, 1 mM $NaHCO_3$, 10 mM NaCl, 20°C, 260 rpm, pH 8.0±0.2).

An increase in PBSAC dosage resulted in a significant decrease in uranium concentration, even though the surface area of PBSAC was in excess at low dosage (Figure 2A). A dosage of 10 g/L PBSAC (MKD 450) was required to reach the WHO guideline (30 µg/L (WHO, 2017)), corresponding to a removal of 92%. This is higher than the achieved removal (70-80%) with conventional activated carbon using the same adsorbent dosage of 10 g/L (Donat and Erden, 2017), which can be attributed to affinity or boundary layer diffusion. The decrease in q_e with PBSAC dose suggests that either the surface area is a limiting factor or the adsorption of uranium is slow (Figure 2C). MKD 200, at 2 – 10 g/L, and MKD 450, at 0.1 to 10 g/L PBSAC dose indeed took about 1 to 7 hours to reach the equilibrium, whereas MKD 200 at 0.1 to 0.5 g/L took longer (>10 hours) (Figure S10).

The kinetic rate constant (k) (equivalent to the speed of the adsorption reaction) increased with the PBSAC dose (Figure 2D). This was due to the availability of a larger surface area with increased PBSAC dose and ultimately more accessible active sites and faster adsorption. At 10 g/L, the k value

for MKD 200 is comparable to conventional activated carbon (~2 1/h (Abd El-Magied *et al.*, 2021)), while a higher value was obtained with MKD 450 of a larger surface area (Table 2).

Adsorption kinetics revealed that the adsorption is determined by surface adsorption, while ToF-SIMS confirmed the relatively slow advancement of pore diffusion inside the PBSAC. The next section investigates the role of material properties for surface adsorption through variable surface oxygen content of the PBSAC.

3.3. Kinetics of uranium adsorption with PBSAC at a varied surface oxygen content

To further confirm that surface adsorption is the rate-limiting step in the adsorption of uranium with PBSAC, adsorption kinetics were investigated at varied surface oxygen content in PBSAC (Figure 3). The pseudo-first-order fitting is shown in Figure S14, while the parameters can be found in Table S7.

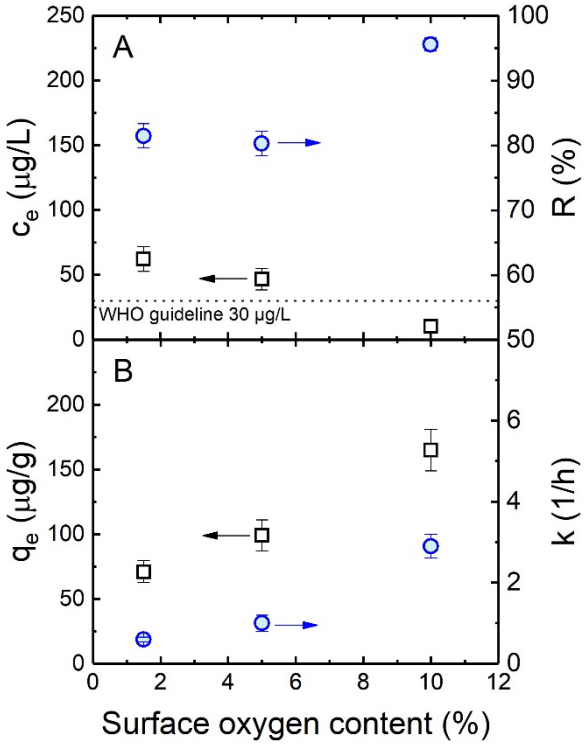

Figure 3. (A) Uranium equilibrium concentration and removal, (B) the kinetic q_e and k using 1g/L PBSAC as a function of surface oxygen content (c_0 250 µgU/L, 1 mM $NaHCO_3$, 10 mM NaCl, 20°C, 260 rpm, pH 8.0±0.2).

When increasing the surface oxygen content from 1.5 to 10%, the uranium concentration at equilibrium dropped from 62 to 10 µgU/L achieving the WHO guideline (Figure 3A) at what conditions – these statements are a bit too general. Similarly, uranium removal increased from 81 to

96% with increasing surface oxygen content (Figure 3A). Following the same trend, uranium uptake at equilibrium almost doubled and increased from 71 to 165 µg/g. Surface oxygen content plays an important role in surface adsorption, particularly in the presence of an affinity to oxygen-containing functional groups (Fan *et al.*, 2018; Yu *et al.*, 2014; Yu *et al.*, 2015). This is the case for PBSAC, where uranium adsorption on the surface could be enhanced through an increase in the carboxyl group moieties (Tagliavini *et al.*, 2017). Hence, it enhances short-range interactions, including hydrogen bonding, van der Waals forces, and anion-π interaction with the uranyl carbonate complexes (Guo *et al.*, 2021; Xie *et al.*, 2019).

Assuming fixed surface area and pore characteristics at identical activation levels (Table 2), the faster surface adsorption of uranium onto the surface of the PBSAC can be attributed to the increased surface oxygen content. This faster adsorption rate at 10% oxygen content was obtained is shown in Figure 3B. This could be due to enhanced short-range interactions, including hydrogen bonding, van der Waals forces, and anion-π interaction with the uranyl carbonate complexes (Guo *et al.*, 2021; Xie *et al.*, 2019). In this case, surface adsorption, which is a common transport mechanism in activated carbon (Worch, 2021), appears to be the rate-limiting step in the adsorption of uranium onto PBSAC. The adsorption capacity of PBSAC is now investigated with the Langmuir isotherm model.

3.4. Isotherms of uranium adsorption with PBSAC

The adsorption capacity of PBSAC before saturation, along with kinetics, was investigated by employing the Langmuir isotherm (Figure 4). The adsorption intensity at different uranium initial concentrations was visualised by ToF-SIMS analysis (Figure 4E). Concentration, uptake, and removal of uranium as a function of time and pseudo-first-order fitting parameters can be found in Figure S15 and Table S8.

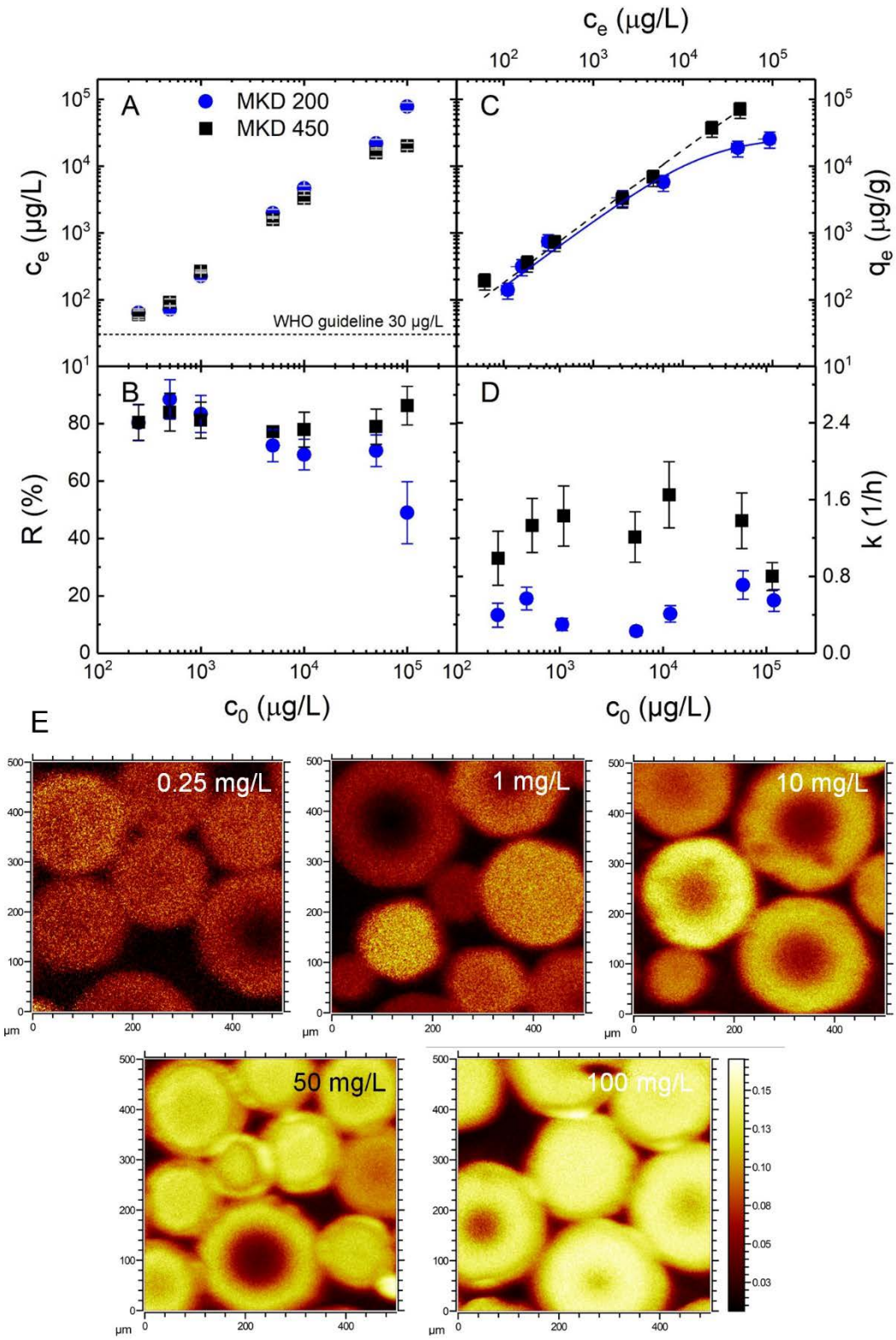

Figure 4. (A) uranium equilibrium concentration (c_e), (B) uranium removal, (C) uranium uptake at equilibrium as a function of c_e, and (D) k as a function of initial concentration (c_0) at 1 g/L of MKD 200 and MKD 450. (E) ToF-SIMS images of MKD 200 showing adsorbed UO_2^{2+} at equilibrium (exposure time of 26 h) (c_0 0.25 to 100 mgU/L, 1 mM $NaHCO_3$, 10 mM NaCl, 20◦C, 260 rpm, pH 8.0±0.3). The lines in (C) show the Langmuir model fit.

The equilibrium concentration increased with the initial concentration of uranium (Figure 4A), and with the overlapping error bars, the removal of uranium was in the range of 71–88 % (Figure 4B).

However, at high uranium concentrations (100 mgU/L) MKD 200 dropped to 50%. The uptake at equilibrium (q_e) increased with equilibrium concentration (Figure 4C). The saturation could not be observed for both MKD 450 at c_0 from 0.25 to 100 mgU/L, while MKD 200 was close to reaching saturation at 100 mgU/L (Figure 4C). Higher initial concentrations (higher than 100 mgU/L) could not be investigated due to radiation safety rules regarding uranium handling that impose strict limits on the storage and handling of radioactive materials including depleted uranium. The Langmuir isotherm fitted well, and the determined maximum adsorption capacity (q_m) of 28 mgU/g for MKD 200 and 667 mg/g for MKD 450 (Table S7). The q_m for MKD 450 is significantly higher than what has been reported for conventional AC (25 to 79 mgU/g; Table S1), and even higher than some recent functionalized carbon-based adsorbents (up to 617.2; Table S1). The comparison with other inorganic and carbon-based adsorbents can be found in Table S1. The independence of the kinetic rate constant to the initial concentration of uranium, considering the overlapping error bars, was expected as predicted by pseudo-first-order theory (Tran *et al.*, 2017b).

The trend of the adsorbed mass at equilibrium could be observed with ToF-SIMS images (Figure 4E), in which the uranium signal increases with elevated initial uranium concentration (also see Figure S9 for pixel-resolved uranium content in PBSAC samples). Even PBSAC samples that were saturated (50 and 100 mgU/L; Figure 4), exhibited unoccupied volume that was not accessible to uranium adsorption. This may be the case alike small pore regions found in commercial activated carbon may not even be accessible to argon for BET characterisation (Nguyen and Bhatia, 2012). The saturation time, which was presumably not completely reached for MKD 200, could be another reason that explains the observed unoccupied volume in the PBSAC.

The adsorption mechanism (physical adsorption) will subsequently be confirmed by investigating the role of temperature and adsorption thermodynamics of uranium with PBSAC.

3.5. Thermodynamics of uranium adsorption with PBSAC

Temperature plays an important role in the adsorption of uranium with carbon-based adsorbents (Alahabadi *et al.*, 2020; Yi *et al.*, 2020b). Adsorption experiments were carried out at temperatures between 10 and 80 °C, equilibrium concentration, removal, equilibrium uptake, and kinetic rate constant were investigated (Figure 5). Concentration, uptake, and removal of uranium as a function of time and pseudo-first-order fitting parameters can be found in Figure S16 and Table S10.

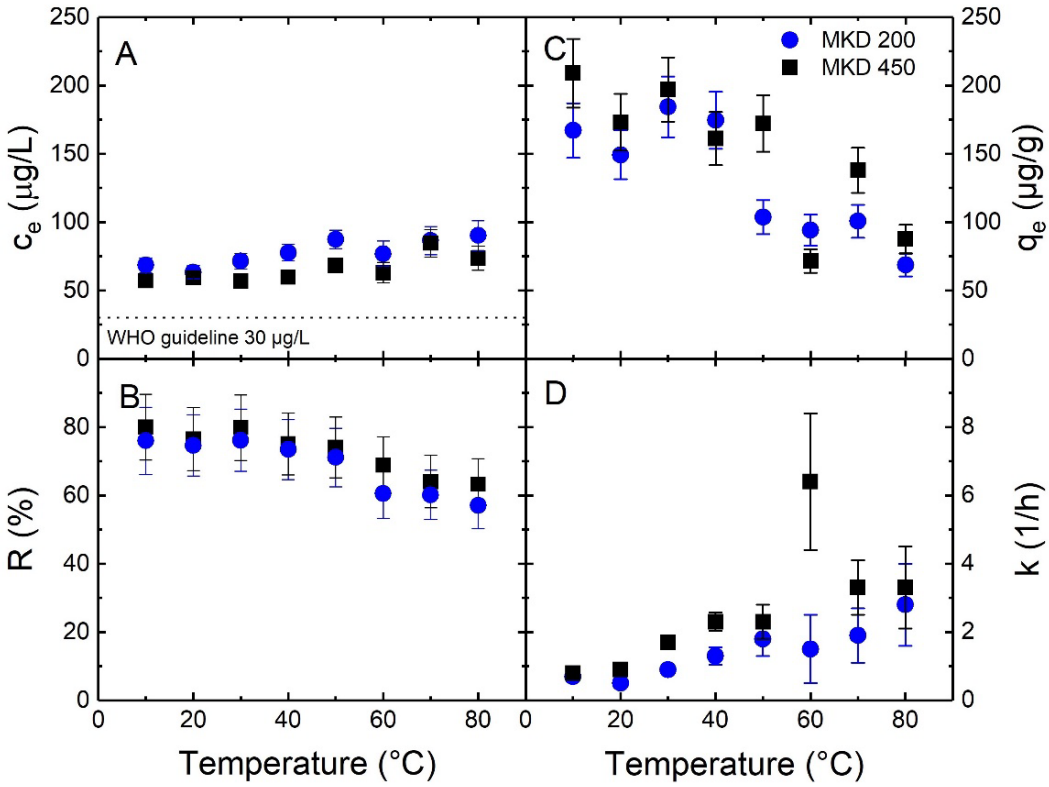

Figure 5. (A) Uranium equilibrium concentration, (B) removal, (C) uranium uptake at equilibrium with their respective (D) k at different temperatures at 1 g/L of MKD 200 and MKD 450 (c_0 250 µgU/L, 1 mM $NaHCO_3$, 10 mM NaCl, 260 rpm, pH 8.0±0.2).

An effect of temperature on equilibrium concentration and removal was within the error (Figure 5A, B). However, the uptake at equilibrium reduced with an increase in temperature (after 40°C) for both MKD 200 and MKD 450 (Figure 5C). Lower adsorption at higher temperatures, which can be due to the increasing Brownian motion of the molecules (Brush, 1968; Jakobsson and Chiu, 1988), is an indication of physical adsorption (Liu, 2009; Worch, 2012). As temperature increases the motion of the uranyl species increases, and this can hinder short-range interactions with the PBSAC surface, such as van der Waals forces. This is also applicable for charged surfaces (unlike PBSAC), in which

Brownian motion can affect the electrical double layer (Syed *et al.*, 2013), and hence the long-range interactions. These explanations are in agreement with previous adsorption studies that discuss the effect of temperature on physical adsorption (Guo and Lua, 2002; Prajapati and Mondal, 2019; Tran *et al.*, 2018). Even though the rate of adsorption k increases with temperature, the desorption rate (not determined in this work) should increase with temperature, particularly for exothermic processes, such as in the case of physical adsorption (Islam *et al.*, 2021). This may indicate that adsorption would be thermodynamically unfavourable at higher temperatures (Erkey and Türk, 2021).

To further confirm the type of the adsorption mechanism between uranium and PBSAC (physical or chemical adsorption), thermodynamic characteristics, including the activation energy (E_a), enthalpy change (ΔH°) and Gibbs free energy change (ΔG°) were investigated (Table 3). These parameters provide information on inherent energetic changes in the adsorption process (Tran *et al.*, 2017b). If physical adsorption was predominant, the process should result in lower magnitudes of ΔH^0 (<40 kJ/mol) and ΔG^0 (–20 to 0 kJ/mol) with a low energy requirement (Inglezakis and Poulopoulos, 2006; Jaerger *et al.*, 2015).

Table 3. Thermodynamic parameters of uranium adsorption with PBSAC with varying temperatures (10 to 80 °C).

PBSAC type	**Thermodynamic parameter**	**Temperature (°C)**							
		10	20	30	40	50	60	70	80
MKD 200	K_d (-)	2	2	3	2	0.7	0.6	0.7	0.4
	ΔG° (kJ/mol)	-18±1	-18±1	-20±2	-20±1	-18±3	-18±3	-19±3	-17±3
	ΔH° (kJ/mol)	-17±3							
	ΔS° (kJ/mol)	48±7							
	E_a (kJ/mol)	21±4							
MKD 450	K_d (-)	5	2	4	2	2	0.4	1.2	0.5
	ΔG° (kJ/mol)	-20±2	-19±2	-21±2	-20±3	-21±3	-17±2	-20±3	-18±3
	ΔH° (kJ/mol)	-21±4							
	ΔS° (kJ/mol)	54±8							
	E_a (kJ/mol)	13±2							

The low magnitude (< 40 kJ/mol) and the negative values (–17 to –21 kJ/mol) of ΔH° indicate an exothermic adsorption process with a relatively lower binding strength (physical adsorption) (Ho and McKay, 1999). The negative value of ΔH° is in agreement with the trend of q_e with temperature, if q_e increases with T, then ΔH° must be positive (Tran *et al.*, 2017b). ΔG° were all negative (between –17 and –21 kJ/mol) and their lower magnitude (0 to –20 kJ/mol) suggested an energetically favourable and spontaneous physical adsorption (Lung *et al.*, 2021). The positive values of ΔS° may indicate that uranium is not restrained at the interface and can diffuse into the pores (LeVan *et al.*, 2008). In addition, ΔS° also reflects the affinity of uranium to PBSAC, suggesting increased randomness in the adsorption process (Al-Ghouti and Da'ana, 2020). E_a (21 and 13 kJ/mol) assumed a value below the activation energy range for chemical adsorption (40 to 800 kJ/mol), which means that the adsorption of uranium to PBSAC is indeed a physical process (Nollet *et al.*, 2003). The E_a (13–21 KJ/mol) obtained is close to the reported range of the adsorption energy (9 to 16 kJ/mol, Table S1) of uranium to activated carbon.

The next section will investigate the role of speciation in the adsorption process. Naturally, speciation changes with pH, and ToF-SIMS analysis can identify surface adsorption and intra-particle adsorption of the different uranium species.

3.6. Role of uranium speciation in adsorption on PBSAC

With the presence of carbonates in the solution, different hydrolysed forms and carbonate complexes are formed for uranium at different pH values (Krestou and Panias, 2004). This can affect adsorption. PBSAC is an uncharged carbonaceous surface (Böhringer *et al.*, 2011), which means that different adsorption behaviours are expected with different uranium species. Equilibrium concentration, removal, equilibrium uptake, and kinetic rate constant of uranium adsorption with PBSAC were investigated at the pH range of 2 to 12 (Figure 6). Concentration, uptake, and removal of uranium as a function of time and pseudo-first-order fitting parameters can be found in Figure S17 and Table S11.

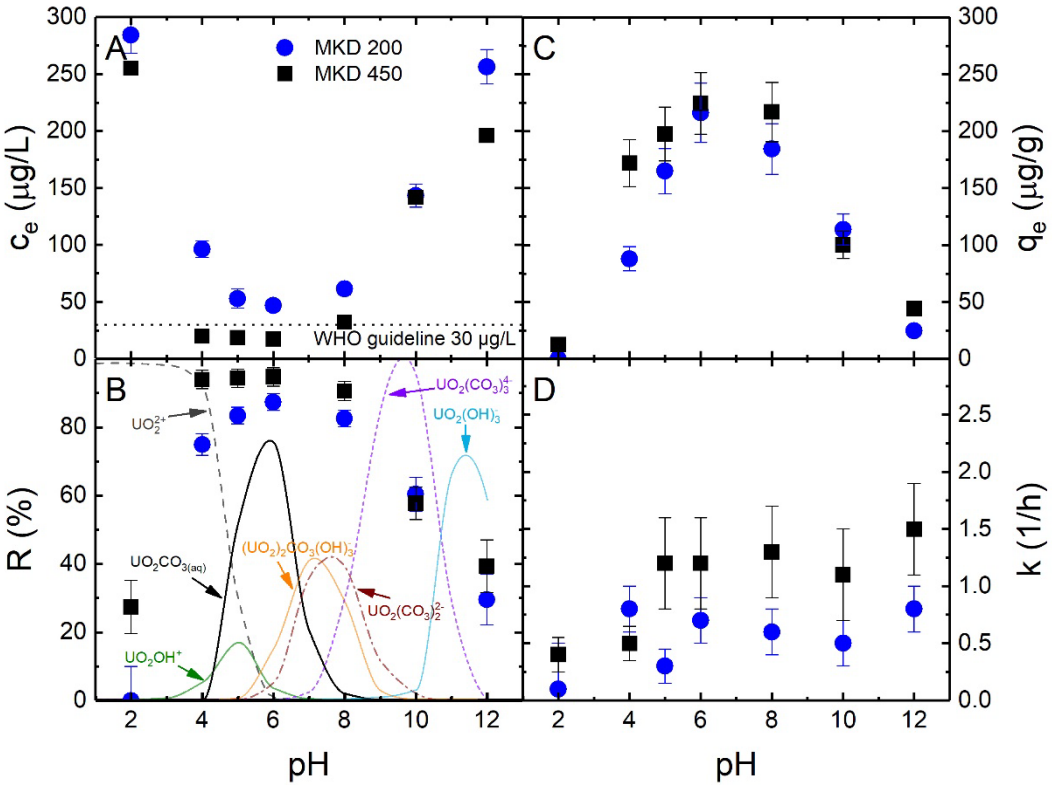

Figure 6. (A) uranium equilibrium concentration, (B) removal, (C) uranium uptake at equilibrium with their respective (D) k as a function of pH at 1 g/L of MKD 200 and MKD 450 (c_0 250 µgU/L, 1 mM $NaHCO_3$, 10 mM NaCl, 260 rpm). Uranium (VI) speciation in (B) was simulated using MINTEQ (V3.1, Sweden) at the corresponding water matrix at 20°C and CO_2 to atmospheric pressure (partial pressure $3.9 \cdot 10^{-4}$ bar).

Equilibrium concentration and removal of uranium were affected by pH, in which the WHO guideline was achieved at the pH range of 4 to 8, considering the error bars (Figure 6A, B). The same trend was observed for uranium adsorption with activated carbon (Donat and Erden, 2017). The highest uptake at equilibrium was obtained at the pH range of 6 to 8 where the species $UO_2CO_{3(aq)}$ predominated the solution together with the anionic uranyl carbonate complexes ($UO_2(CO_3)_2^{2-}$ and $(UO_2)_2CO_3(OH)_3^-$) (Figure 6B). At this pH, the OH groups of the carboxylic acid appeared to favour van der Waals forces, hydrogen bonding and non-covalent π interactions. As the pH increased from 2 to 6, equilibrium uptake increased from 0 to 220 µg/g (for an initial concentration of 250 µgU/L). In the acidic pH range of 2 to 4, unfavourable adsorption of the predominant uranyl ion species (UO_2^{2+}) was observed. In this case, uranium may have few binding sites on the adsorbent surfaces, where the competition of H_3O^+ ions is taking place (Schierz and Zänker, 2009). At pH > 8, the adsorption began to decline to indicate that the species present in this pH range (negative uranium species) had a lower

chance of adsorption onto PBSAC. The presence of the deprotonated carboxylic groups (COO^-), which generally deprotonate from pH 7.4 (Speight, 2005), may have repulsed the negative uranium species and hindered the adsorption of uranium to the surface.

The interaction responsible for adsorption facilitated the adsorption of positive and neutral species and restrained the negative species. As PBSAC is characterised by a neutral surface over pH 2 to 10, with limited oxygen content on the surface (Tagliavini *et al.*, 2017), the short-range van der Waals interactions, together with hydrogen bonding and anion/cation-π interactions, may be responsible for the adsorption of uranium to PBSAC.

To further understand the adsorption behaviour of the different uranium species, PBSAC samples of different pH were analysed by ToF-SIMS upon interlaced sputtering with 1 keV O_2^+ ion beam. ToF-SIMS images of uranium signal as a secondary ion UO_2^+ and the fragmentation ion UO_2^+–R at different pH were identified (Figure 7). The mass spectra for various uranium signals are shown in Figure S7.

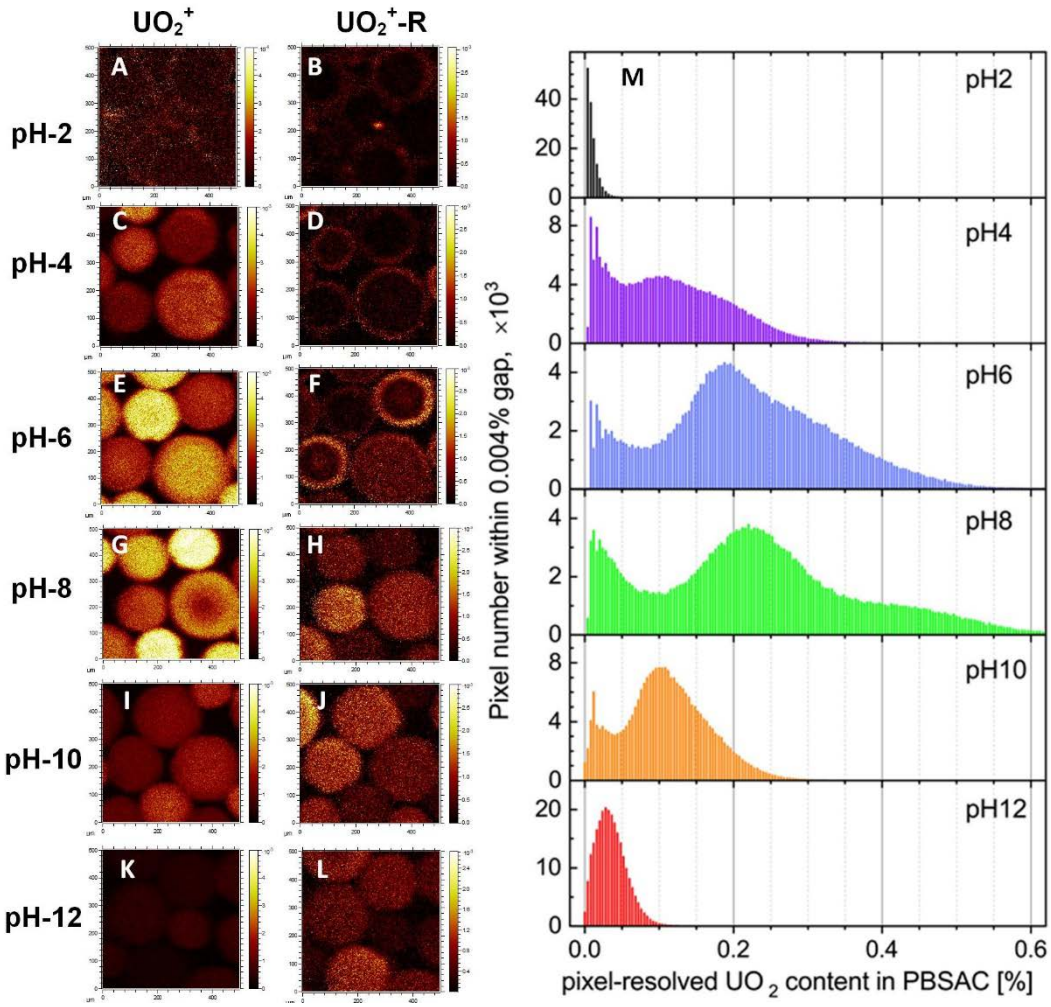

Figure 7. Tof-SIMS images of the secondary ions $UO_2^+$and UO_2^+-R on PBSAC at pH (A, B) 2, (C, D) 4, (E, F) 6, (G, H) 8, (I, J) 10, and (K, L) 12. (M) Pixel resolved UO_2 content at different pH (c_0 250 µgU/L, 1 mM $NaHCO_3$, 10 mM NaCl, 20°C, 260 rpm).

Within the whole pH 2-12 range, UO_2^{2+} ion counts in ToF-SIMS mass spectra originate from uranyl stripped of its coordinating ligands due to strong molecular fragmentation upon sample sputtering with 1 keV O_2^+ ion beam. This detachment of uranyl ligands made UO_2^{2+} ions the major U-representative for all U-speciation revealed and allowed for a rough estimation of pixel-resolved U-content from UO_2^{2+} ion counts normalised to the total ion counts (TIC). The pixel-resolved distribution of U-content (Figure 7) reveals several concentration bands corresponding to various U-speciation available at different pH. At pH 2, UO_2^{2+}, the most abundant species, shows a very high diffusion and weak adsorption resulting in a diffused UO_2^+ distribution pattern. At pH 4-6, carbonate ligands facilitate fast adsorption limiting the uranyl diffusion within the outer PBSAC layers that present in a ring-shaped UO_2-C_2H^+ distribution pattern (Figure 7D, F). This could be attributed to the

interacted $UO_2(OH)^+$ present at pH 4-6 with the surface of the PBSAC, through non-covalent interactions with carboxyl groups, that could not diffuse inside the PBSAC. The maximum amount of adsorbed uranium was observed at pH 6-8. This broadly represents all U-containing groups attached to PBSAC in various ways. At pH 8-12, UO_2^+–R fragments were found in the whole PBSAC together with UO_2^+ fragments (Figure 7. H, J, and L). In this case, UO_2^+–R fragments could be attributed to the surface adsorption and the entrapment of uranyl carbonate complexes inside the PBSAC. This indicates that intra-particle diffusion of uranium is favourable for the uranyl carbonate complexes. Development (and aggregation) of various large-size carbonate ligands at pH 8 may be a reason for a reduced diffusion, resulting in a donut-shaped UO_2^+ distribution pattern. The variety of carbonate ligands is reduced and provides a quasi-homogeneous uranyl diffusion into PBSAC at pH 10. Hydroxyl ligands dominating at pH 12 define the diffusion of uranyl into PBSAC spheres. At pH 12, the homogeneous low yield of UO_2^+ may originate from the residual carbonate-coordinated uranyl as well as from hydroxyl-coordinated one, revealing stronger adsorption compared to UO_2^{2+} at pH 2.

ToF-SIMS analysis revealed that the intra-particle diffusion is selective for the uranyl carbonate complexes, while the adsorption of the uranyl species was mostly limited to surface adsorption. In this process, several mechanisms could be involved in the adsorption, which is discussed in the next section.

3.7. Suggested adsorption and transport mechanisms

According to the previous experimental results on adsorption kinetics, isotherms and thermodynamics, as well as ToF-SIMS analysis of PBSAC samples (time, concentration, and pH series), the potential transport and adsorption mechanisms of uranium on PBSAC are proposed (Figure 8).

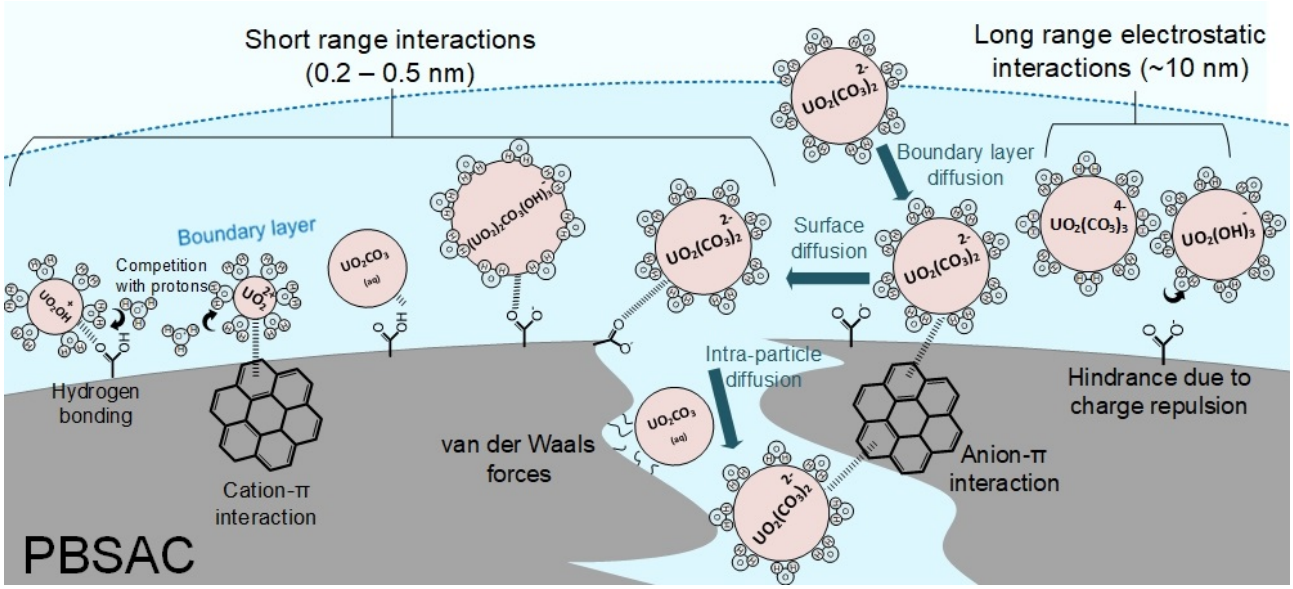

Figure 8. Schematic (not to scale) illustrating the potential mass transfer and adsorption mechanisms of U(VI) species on PBSAC.

Surface adsorption is the rate-limiting step, evidenced by the increase in the kinetic rate constant (k) with increasing oxygen content on the surface of PBSAC. Surface-adsorbed uranium subsequently diffuses towards the core of the PBSAC. These are typical transport mechanisms of adsorbate in activated carbon material, which are known as boundary layer diffusion (or external diffusion), surface diffusion (or film diffusion at the adsorbent surface), and intraparticle diffusion (Sahoo and Prelot, 2020; Tran *et al.*, 2017b). The concentration gradient is the driving force of the different diffusion steps (Wang and Guo, 2020). The internal diffusion has been visualised by ToF-SIMS analysis for time series PBSAC samples, which showed the gradual diffusion of uranium inside the PBSAC over the adsorption time.

Regarding the adsorption mechanisms, the positive uranyl species (UO_2^{2+}, UO_2OH^+) are suggested to be interacting with the PBSAC surfaces through van der Waals forces, π-electron cloud, or/and hydrogen bonding. In the absence of functional groups of protonated functional groups, the ion metals, which includes uranyl cations, tend to adsorb on the π-electron cloud in the basal planes of the surface of AC (Wang *et al.*, 2022b; Yoshihara *et al.*, 2009). Weak van der Waals forces have always been identified as an important contributor to the adsorption mechanism of metals in AC (Kyzas *et al.*, 2019). Furthermore, in carbon materials with carboxyl groups on the surface, uranyl

ions adsorption on the surface can occur via inter/intra-molecular hydrogen bonding (Kannan *et al.*, 2017; Wu *et al.*, 2014). This could explain why UO_2^{2+} species were limited to surface adsorption at pH 2 as evidenced by ToF-SIMS. The presence of H_3O^+ ions can compete with the uranyl cations to exhibit the previous adsorption mechanisms (Schierz and Zänker, 2009), which explains the low adsorption obtained at pH 2-4. Charge interactions, on the other hand, are unlikely because, at the pH conditions favouring the formation of uranyl cations species (pH 2-4), the carboxyl groups that may exist on the PBSAC surface are not protonated yet, while Tagliavini *et al.* (2017) have reported an overall neutrally charged surface of the PBSAC, which makes this mechanism unlikely.

In the presence of the negative uranyl carbonate complexes (at pH > 7), van der Waals forces together with anion-π interactions and hydrogen bonding could be responsible for the adsorption mechanisms. Such weak and short-range interactions were evidenced by thermodynamic parameters, which showed that the adsorption process is reversible physical adsorption from forces with lower binding energy (13 – 21 kJ/mol). By increasing the pH to 12, the adsorption of the negative uranyl carbonate complexes is probably hindered by the deprotonated OH on the surface of the PBSAC, which can cause charge repulsion, which is a long-range interaction, with the negatively charged uranyl carbonate complexes. However, ToF-SIMS images at pH 10-12 revealed that uranium was inside the PBSAC pores, which indicates that short-range interactions may have still occurred at this pH range. The irrelevance of the charge repulsion and the absence of proton competition favoured the adsorption of the neutral species $UO_2CO_{3(aq)}$ to PBSAC, which predominates the solution at pH 6.

Uranium removal by PBSAC adsorption is ideal for contaminated natural water sources with a pH of 6-7, because of the predominance of uranyl carbonate species. However, the presence of calcium or magnesium (responsible for water hardness), which can form ternary complexes with uranyl carbonates (Smedley and Kinniburgh, 2023), or the presence of competing metal cations such as iron may interfere with adsorption (Yakout and Abdeltawab, 2015). Therefore, the removal of uranium with PBSAC adsorption was investigated using real water contaminated with U.

3.8. Uranium removal from natural water using PBSAC

The performance, in terms of uranium concentration and removal, of PBSAC was investigated in natural water conditions. For this, spring water with naturally loaded uranium from St. Blasien-Menzenschwand in the Waldshut region in Baden-Württemberg (Germany) (Figure S1), was treated with MKD 200 at 1g/L, which was later visualised with ToF-SIMS (Figure 9). The water quality of the real water is summarised in Table S2.

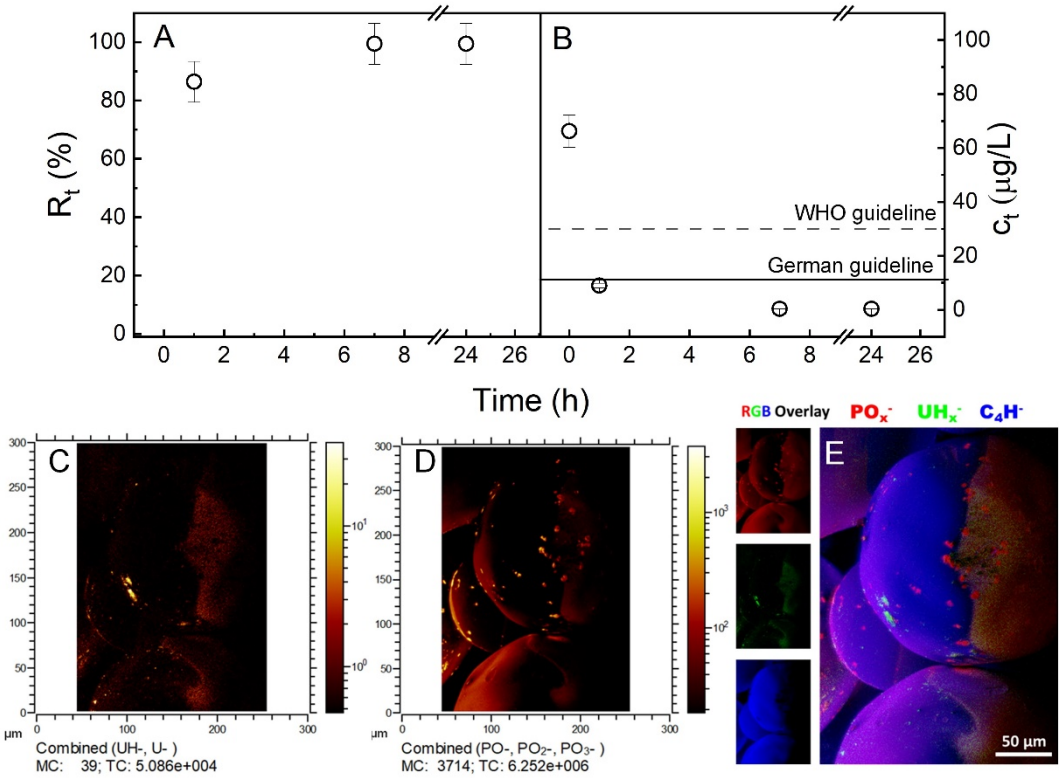

Figure 9. (A) Removal and (B) supernatant concentration as a function of adsorption time. ToF-SIMS elemental distribution images of (C) uranium, (D) phosphate, and (E) the overlay of uranium (green), phosphate (red), and carbon (blue) on MKD 200 with adsorbed uranium from real water (c_0 67 µg/L uranium, pH 6.7, PBSAC 1 g/L, 260 rpm, 26 h, and 20°C).

Removal of uranium from the contaminated spring water was 99 %, resulting in a uranium concentration of 0.7 µg/L, which is well below the WHO guideline (30 µg/L; (WHO, 2017)) and the German guideline (10 µg/L; (Banning and Benfer, 2017)) (Figure 9A, B). The presence of potential competing inorganics such as arsenic (Table S2), which can also adsorb to PBSAC (Schrage *et al.*, 2014), appears to not interfere with the adsorption of uranium. However, the presence of organic matter, which was not present in this particular natural water, could be a strong inhibitor of uranium

adsorption in activated carbon (Yakout *et al.*, 2013). This may require further investigation even though Wolters *et al.* (2019) reported that PBSAC was resilient to organic matter interference.

ToF-SIMS analysis revealed that uranium was found distributed on the surface (less intense) of the PBSAC sample (MKD 200) and at specific hotspots in higher amounts, which could be attributed to oxygen-containing functional groups on the PBSAC surface (Figure 9C). It is expected that adsorbed uranium diffuses into the pores (as evidenced by ToF-SIMS) leaving less uranium on the surface. Interestingly, adsorbed phosphate was detected at different hotspots across the surface, which could be attributed to uranium phosphate complexes (Smedley and Kinniburgh, 2023). However, its adsorption on the PBSAC was not due to its complexation with uranium, since the phosphate hotspots did not coexist with the uranium hotspots, as shown by the ToF-SIMS (Figure 9D, E).

4. Conclusions

The static adsorption experiments showed that PBSAC (at 1 g/L dosage) exhibited a slow equilibrium time (7 to 24 hours) to achieve an equilibrium uptake of 185±20 µg/g from an initial concentration of 250 µgU/L at pH 8.0±0.3. To reach the WHO guideline (30 µgU/L) under the same conditions, 10 g/L of PBSAC dosage or increasing surface oxygen content from 1.5 to 10% with 1 g/L PBSAC dosage was required.

The Langmuir isotherm revealed a maximum adsorption capacity of 28 mg/g for MKD 200 and 667 mg/g for MKD 450, while the thermodynamics showed that the adsorption process was physical with an adsorption energy of 13 to 21 kJ/mol.

Water chemistry (pH) had a significant effect on adsorption due to uranium speciation, where pH 6-8 was found to be the most favourable condition for uranium adsorption. ToF-SIMS analysis could identify the adsorption of the different uranium species on the surface or/and inside the mesoporous structure of the PBSAC due to intraparticle diffusion. The adsorption of uranyl cations was limited to surface adsorption, while the uranyl carbonate complexes were visualised inside the PBSAC. The

adsorption of the different uranium species could be due to weak interactions with low binding strength, corresponding to van der Waals, anion/cation-π, and hydrogen bonding interactions.

Treatment of contaminated spring water with PBSAC was successful, in that both WHO and German guidelines for drinking water were met. PBSAC can also be tailored to further improve the adsorption properties and could be used to develop hybrid adsorption-assisted membrane treatment technology for uranium removal.

5. Acknowledgements

The Helmholtz Association Recruitment Initiative and Helmholtz-ERC Recognition Award (HGF ERC-RA0032) are acknowledged for providing funding to IAMT-KIT. Katholischer Akademischer Ausländer Dienst (KAAD) granted a PhD scholarship for J. Joseph. Thomas Spiegelhalter (Radon Revital Bad, Menzenschwand, Germany) is thanked for providing access to real water samples. Gerhard Frank, Danica Melzer, and Motasem Alshaar, from the Office of Safety and Environment (SUM) in KIT, facilitated technical regulation, health, and safety measures for working with uranium in IAMT-KIT. Dr.-Ing. Minh Nhat Nguyen (IAMT-KIT) is thanked for his explanations of the supramolecular adsorption mechanism. The authors acknowledge Dr. Matthias Schmidt (UFZ) for providing helium-ion micrographs and energy-dispersive X-rays spectrometry data of PBSAC and critical discussions on the manuscript. The support from the Helmholtz Centre for Environmental Research–(UFZ) provided to the ProVIS Centre for Chemical Microscopy and the funds for ProVIS establishment through the Europäischer Fonds für regionale Entwicklung (EFRE) and the Freistaat Sachsen Program are greatly acknowledged.

6. Supporting information

Supplementary data related to this article is available in the supporting information (SI) section. The SI contains further results as figures with comments about: (i) the application of carbon-based materials for uranium adsorption; (ii) the water quality of the Menzenschwand water samples; (iii) calibration and limit of detection of the analytical methods; (iv) error analysis; (v) sample preparation

and supplementary information about the ToF-SIMS method used in this work; and (vi) kinetics and isotherm model parameters at varied operational conditions and PBSAC material characteristics.

7. References

Aaberg, M., Ferri, D., Glaser, J., Grenthe, I., 1983. Structure of the hydrated dioxouranium(VI) ion in aqueous solution. An x-ray diffraction and proton NMR study. Inorganic Chemistry 22(26), 3986-3989.

Abd El-Magied, M.O., Hassan, A.M., El-Aassy, I.K., Gad, H.M.H., Youssef, M.A.M., Mohammaden, T.F., 2021. Development of functionalized activated carbon for uranium removal from groundwater. International Journal of Environmental Research 15(3), 543-558.

Al-Ghouti, M.A., Da'ana, D.A., 2020. Guidelines for the use and interpretation of adsorption isotherm models: A review. Journal of Hazardous Materials 393, 122383.

Alahabadi, A., Singh, P., Raizada, P., Anastopoulos, I., Sivamani, S., Dotto, G.L., Landarani, M., Ivanets, A., Kyzas, G.Z., Hosseini-Bandegharaei, A., 2020. Activated carbon from wood wastes for the removal of uranium and thorium ions through modification with mineral acid. Colloids and Surfaces A: Physicochemical and Engineering Aspects 607, 125516.

Alam, M.S., Cheng, T., 2014. Uranium release from sediment to groundwater: Influence of water chemistry and insights into release mechanisms. Journal of contaminant hydrology 164, 72-87.

Amini, A., Khajeh, M., Oveisi, A.R., Daliran, S., Ghaffari-Moghaddam, M., Delarami, H.S., 2021. A porous multifunctional and magnetic layered graphene oxide/3D mesoporous MOF nanocomposite for rapid adsorption of uranium(VI) from aqueous solutions. Journal of Industrial and Engineering Chemistry 93, 322-332.

Amrute, A.P., Krumeich, F., Mondelli, C., Pérez-Ramírez, J., 2013. Depleted uranium catalysts for chlorine production. Chemical Science 4(5), 2209-2217.

Ansoborlo, E., Lebaron-Jacobs, L., Prat, O., 2015. Uranium in drinking-water: A unique case of guideline value increases and discrepancies between chemical and radiochemical guidelines. Environment International 77, 1-4.

Aslani, C.K., Amik, O., 2021. Active Carbon/PAN composite adsorbent for uranium removal: Modeling adsorption isotherm data, thermodynamic and kinetic studies. Applied Radiation and Isotopes 168, 109474.

Bakhsh, E.M., Khan, S.B., Akhtar, K., Danish, E.Y., Fagieh, T.M., Qiu, C., Sun, Y., Romanovski, V., Su, X., 2022. Simultaneous preparation of humic acid and mesoporous silica from municipal sludge and their adsorption properties for U(VI). Colloids and Surfaces A: Physicochemical and Engineering Aspects 647, 129060.

Banning, A., Benfer, M., 2017. Drinking water uranium and potential health effects in the German federal state of Bavaria.

Bastrakov, E., Jaireth, S., Mernagh, T., 2010. Solubility of uranium in hydrothermal fluids at 25-300 °c. Implications for the formation of uranium deposits. Geosci. Aust. Rec. 2010.

Belgacem, A., Rebiai, R., Hadoun, H., Khemaissia, S., Belmedani, M., 2014. The removal of uranium (VI) from aqueous solutions onto activated carbon developed from grinded used tire. Environmental Science and Pollution Research 21(1), 684-694.

Benettoni, P., Stryhanyuk, H., Wagner, S., Kollmer, F., Moreno Osorio, J.H., Schmidt, M., Reemtsma, T., Richnow, H.-H., 2019. Identification of nanoparticles and their localization in algal biofilm by 3D-imaging secondary ion mass spectrometry. Journal of Analytical Atomic Spectrometry 34(6), 1098-1108.

Betti, M., 2003. Civil use of depleted uranium. Journal of Environmental Radioactivity 64(2), 113-119.

Bhalara, P.D., Punetha, D., Balasubramanian, K., 2014. A review of potential remediation techniques for uranium(VI) ion retrieval from contaminated aqueous environment. Journal of Environmental Chemical Engineering 2(3), 1621-1634.

Blanchard, G., Maunaye, M., Martin, G., 1984. Removal of heavy metals from waters by means of natural zeolites. Water Research 18(12), 1501-1507.

Böhringer, B., Guerra Gonzalez, O., Eckle, I., Müller, M., Giebelhausen, J.-M., Schrage, C., Fichtner, S., 2011. Polymer-based spherical activated carbons – From adsorptive properties to filter performance. Chemie Ingenieur Technik 83(1-2), 53-60.

Bone, S.E., Cliff, J., Weaver, K., Takacs, C.J., Roycroft, S., Fendorf, S., Bargar, J.R., 2020. Complexation by organic matter controls uranium mobility in anoxic sediments. Environmental Science & Technology 54(3), 1493-1502.

Brush, S.G., 1968. A history of random processes: I. Brownian movement from Brown to Perrin. Archive for History of Exact Sciences 5(1), 1-36.

Caccin, M., Giacobbo, F., Da Ros, M., Besozzi, L., Mariani, M., 2013. Adsorption of uranium, cesium and strontium onto coconut shell activated carbon. Journal of Radioanalytical and Nuclear Chemistry 297(1), 9-18.

Calì, E., Qi, J., Preedy, O., Chen, S., Boldrin, D., Branford, W.R., Vandeperre, L., Ryan, M.P., 2018. Functionalised magnetic nanoparticles for uranium adsorption with ultra-high capacity and selectivity. Journal of Materials Chemistry A 6(7), 3063-3073.

Catalano, J.G., McKinley, J.P., Zachara, J.M., Heald, S.M., Smith, S.C., Brown, G.E., 2006. Changes in uranium speciation through a depth sequence of contaminated hanford sediments. Environmental Science & Technology 40(8), 2517-2524.

Chen, S., Koshy, D.M., Tsao, Y., Pfattner, R., Yan, X., Feng, D., Bao, Z., 2018. Highly tunable and facile synthesis of uniform carbon flower particles. Journal of the American Chemical Society 140(32), 10297-10304.

Chingombe, P., Saha, B., Wakeman, R.J., 2005. Surface modification and characterisation of a coal-based activated carbon. Carbon 43(15), 3132-3143.

Craft, E.S., Abu-Qare, A.W., Flaherty, M.M., Garofolo, M.C., Rincavage, H.L., Abou-Donia, M.B., 2004. DEPLETED AND NATURAL URANIUM: CHEMISTRY AND TOXICOLOGICAL EFFECTS. Journal of Toxicology and Environmental Health, Part B 7(4), 297-317.

Donat, R., Erden, K.E., 2017. Adsorption of U(VI) ions from aqueous solutions by activated carbon prepared from Antep pistachio (Pistacia vera L.) shells. Radiochimica Acta 105(5), 359-367.

Duan, J., Ji, H., Xu, T., Pan, F., Liu, X., Liu, W., Zhao, D., 2021. Simultaneous adsorption of uranium(VI) and 2-chlorophenol by activated carbon fiber supported/modified titanate nanotubes (TNTs/ACF): Effectiveness and synergistic effects. Chemical Engineering Journal 406, 126752.

El-Sayed, A.A., 2008. Kinetics and thermodynamics of adsorption of trace amount of uranium on activated carbon. 96(8), 481-486.

Endrizzi, F., Rao, L., 2014. Chemical speciation of uranium(VI) in marine environments: Complexation of calcium and magnesium ions with $[(UO_2)(CO_3)_3]^{4-}$ and the effect on the extraction of uranium from seawater. Chemistry – A European Journal 20(44), 14499-14506.

EPA, 2007. Technology reference guide for radioactively contaminated media (https://www.epa.gov/sites/default/files/2015-05/documents/media.pdf access date 30/8/2022), Office of radiation and indoor air radiation protection program - United States Environmental Protection Agency.

EPA USA, 2018. 2018 edition of the drinking water standards and health advisories (https://www.epa.gov/sites/default/files/2018-03/documents/dwtable2018.pdf accessed date 4/8/2021), Office of Water U.S. Environmental Protection Agency, Washington, DC.

Erkey, C., Türk, M., 2021. Chapter 6 - Thermodynamics and kinetics of adsorption of metal complexes on surfaces from supercritical solutions. In: Erkey, C., Türk, M. Supercritical fluid science and technology, Elsevier, 2021, pp. 73-127.

Fan, F.-L., Qin, Z., Bai, J., Rong, W.-D., Fan, F.-Y., Tian, W., Wu, X.-L., Wang, Y., Zhao, L., 2012. Rapid removal of uranium from aqueous solutions using magnetic Fe3O4@SiO2 composite particles. Journal of Environmental Radioactivity 106, 40-46.

Fan, Q., Sun, J., Chu, L., Cui, L., Quan, G., Yan, J., Hussain, Q., Iqbal, M., 2018. Effects of chemical oxidation on surface oxygen-containing functional groups and adsorption behavior of biochar. Chemosphere 207, 33-40.

Freundlich, H., 1907. Über die Adsorption in Lösungen. Zeitschrift für Physikalische Chemie 57U(1), 385-470.

Götz, C., Geipel, G., Bernhard, G., 2011. The influence of the temperature on the carbonate complexation of uranium(VI): a spectroscopic study. Journal of Radioanalytical and Nuclear Chemistry 287(3), 961-969.

Grenthe, I., Fuger, J., Lemire, R.J., Muller, A.B., Nguyen-Trung Cregu, C., Wanner, H., 1992. Chemical thermodynamics of uranium, Elsevier Science Publishers, Netherlands.

Grenthe, I., Gaona, X., Plyasunov, A.V., Rao, L., Runde, W.H., Grambow, B., Konings, R.J.M., Smith, A.L., Moore, E.E., 2021. Second update on the chemical thermodynamics of uranium, neptunium, plutonium, americium and technetium, OECD Publishing, Paris.

Guo, H., Mei, P., Xiao, J., Huang, X., Ishag, A., Sun, Y., 2021. Carbon materials for extraction of uranium from seawater. Chemosphere 278, 130411.

Guo, J., Lua, A.C., 2002. Microporous Activated Carbons Prepared from Palm Shell by Thermal Activation and Their Application to Sulfur Dioxide Adsorption. Journal of Colloid and Interface Science 251(2), 242-247.

Guo, X., Wang, J., 2019. A general kinetic model for adsorption: Theoretical analysis and modeling. Journal of Molecular Liquids 288, 111100.

Han, G., Wen, S., Wang, H., Feng, Q., 2020. Selective adsorption mechanism of salicylic acid on pyrite surfaces and its application in flotation separation of chalcopyrite from pyrite. Separation and Purification Technology 240, 116650.

Haynes, W.M., 2016. CRC handbook of chemistry and physics, CRC press.

Health-Canada, 2017. Guidelines for Canadian drinking water quality—summary table, Ottawa, Ontario.

Ho, Y.S., McKay, G., 1999. Pseudo-second order model for sorption processes. Process Biochemistry 34(5), 451-465.

Hu, H., Zhang, X., Wang, T., Sun, L., Wu, H., Chen, X., 2018. Bamboo (Acidosasa longiligula) shoot shell biochar: its potential application to isolation of uranium(VI) from aqueous solution. Journal of Radioanalytical and Nuclear Chemistry 316(1), 349-362.

Hu, T., Ding, S., Deng, H., 2016. Application of three surface complexation models on U(VI) adsorption onto graphene oxide. Chemical Engineering Journal 289, 270-276.

Huang, C., Feng, M., Zhu, X., Zhou, Q., Zeng, S., Huang, Y., Zhang, H., 2021. Polymer precursor strategy toward the precise synthesis of uniform hairy carbon dots with tunable sizes and size effects over their fluorescence. Macromolecules 54(24), 11497-11507.

Inglezakis, V.J., Poulopoulos, S.G., 2006. 2 - Adsorption, ion exchange, and catalysis. In: Inglezakis, V.J., Poulopoulos, S.G. Adsorption, ion exchange, and catalysis, Elsevier, Amsterdam, 2006, pp. 31-56.

Inglezakis, V.J., Zorpas, A.A., 2012. Heat of adsorption, adsorption energy and activation energy in adsorption and ion exchange systems. Desalination and Water Treatment 39(1-3), 149-157.

Islam, M.A., Chowdhury, M.A., Mozumder, M.S.I., Uddin, M.T., 2021. Langmuir adsorption kinetics in liquid media: Interface reaction model. ACS Omega 6(22), 14481-14492.

Israelachvili, J.N., 2011. Chapter 13 - Van der Waals forces between particles and surfaces. In: Israelachvili, J.N. Intermolecular and surface forces (3rd edition), Academic Press, Boston, 2011, pp. 253-289.

Jaerger, S., dos Santos, A., Fernandes, A.N., Almeida, C.A.P., 2015. Removal of p-nitrophenol from aqueous solution using brazilian peat: Kinetic and thermodynamic studies. Water, Air, & Soil Pollution 226(8), 236.

Jakobsson, E., Chiu, S., 1988. Application of Brownian motion theory to the analysis of membrane channel ionic trajectories calculated by molecular dynamics. Biophysical journal 54(4), 751-756.

John Presin Kumar, A., Sivakumar, S., Prasanth, D., Guhanesh, B., Ijas Ahamed, A., 2021. A review on the synthesis of activated carbon from natural resources for mechanical applications.

Vijayan, S., Subramanian, N., Sankaranarayanasamy, K. (eds), pp. 1013-1025, Springer Singapore, Singapore.

Julien, F., Baudu, M., Mazet, M., 1998. Relationship between chemical and physical surface properties of activated carbon. Water Research 32(11), 3414-3424.

Jun, B.-M., Lee, H.-K., Park, S., Kim, T.-J., 2021. Purification of uranium-contaminated radioactive water by adsorption: A review on adsorbent materials. Separation and Purification Technology 278, 119675.

Kannan, S., Kumar, M., Sadhu, B., Jaccob, M., Sundararajan, M., 2017. Unusual intramolecular CH⋯O hydrogen bonding interaction between a sterically bulky amide and uranyl oxygen. Dalton Transactions 46(48), 16939-16946.

Karan, S., Jiang, Z., Livingston, A.G., 2015. Sub–10 nm polyamide nanofilms with ultrafast solvent transport for molecular separation. Science 348(6241), 1347-1351.

Kerisit, S., Liu, C., 2010. Molecular simulation of the diffusion of uranyl carbonate species in aqueous solution. Geochimica et Cosmochimica Acta 74(17), 4937-4952.

Krawczyk-Bärsch, E., Gerber, U., Müller, K., Moll, H., Rossberg, A., Steudtner, R., Merroun, M.L., 2018. Multidisciplinary characterization of U(VI) sequestration by *Acidovorax facilis* for bioremediation purposes. Journal of Hazardous Materials 347, 233-241.

Krestou, A., Panias, D., 2004. Uranium (VI) speciation diagrams in the $UO_2^{2+}/CO_3^{2-}/H_2O$ system at 25° C. European Journal of Mineral Processing & Environmental Protection 4(2).

Kütahyalı, C., Eral, M., 2004. Selective adsorption of uranium from aqueous solutions using activated carbon prepared from charcoal by chemical activation. Separation and Purification Technology 40(2), 109-114.

Kütahyalı, C., Eral, M., 2010. Sorption studies of uranium and thorium on activated carbon prepared from olive stones: Kinetic and thermodynamic aspects. Journal of Nuclear Materials 396(2), 251-256.

Kyzas, G.Z., Bomis, G., Kosheleva, R.I., Efthimiadou, E.K., Favvas, E.P., Kostoglou, M., Mitropoulos, A.C., 2019. Nanobubbles effect on heavy metal ions adsorption by activated carbon. Chemical Engineering Journal 356, 91-97.

Lagergren, S.K., 1898. About the theory of so-called adsorption of soluble substances. Sven. Vetenskapsakad. Handingarl 24, 1-39.

Langmuir, I., 1918. the adsorption of gases on plane surfaces of glass, mica and platinum. Journal of the American Chemical Society 40(9), 1361-1403.

Lapworth, D.J., Brauns, B., Chattopadhyay, S., Gooddy, D.C., Loveless, S.E., MacDonald, A.M., McKenzie, A.A., Muddu, S., Nara, S.N.V., 2021. Elevated uranium in drinking water sources in basement aquifers of southern India. Applied Geochemistry 133, 105092.

LeVan, M.D., Carta, G., Yon, C.M., 2008. Section 16: Adsorption and ion exchange. In: 8th Perry's chemical engineers' handbook, McGraw-Hill, 2008, pp.

Liu, Y., 2009. Is the free energy change of adsorption correctly calculated? Journal of Chemical & Engineering Data 54(7), 1981-1985.

Liu, Y., Shen, L., 2008. From Langmuir kinetics to first- and second-order rate equations for adsorption. Langmuir 24(20), 11625-11630.

Lung, I., Soran, M.-L., Stegarescu, A., Opris, O., Gutoiu, S., Leostean, C., Lazar, M.D., Kacso, I., Silipas, T.-D., Porav, A.S., 2021. Evaluation of CNT-COOH/MnO_2/Fe_3O_4 nanocomposite for ibuprofen and paracetamol removal from aqueous solutions. Journal of Hazardous Materials 403, 123528.

Ma, F., Gui, Y., Liu, P., Xue, Y., Song, W., 2020a. Functional fibrous materials-based adsorbents for uranium adsorption and environmental remediation. Chemical Engineering Journal 390, 124597.

Ma, M., Wang, R., Xu, L., Xu, M., Liu, S., 2020b. Emerging health risks and underlying toxicological mechanisms of uranium contamination: Lessons from the past two decades. Environment International 145, 106107.

Mahadevi, A.S., Sastry, G.N., 2013. Cation−π interaction: Its role and relevance in chemistry, biology, and material science. Chemical Reviews 113(3), 2100-2138.

McKay, G., Otterburn, M.S., Sweeney, A.G., 1980. The removal of colour from effluent using various adsorbents—III. Silica: Rate processes. Water Research 14(1), 15-20.

Mellah, A., Chegrouche, S., Barkat, M., 2006. The removal of uranium(VI) from aqueous solutions onto activated carbon: Kinetic and thermodynamic investigations. Journal of Colloid and Interface Science 296(2), 434-441.

Mellah, A., Chegrouche, S., Barkat, M., 2007. The precipitation of ammonium uranyl carbonate (AUC): Thermodynamic and kinetic investigations. Hydrometallurgy 85(2), 163-171.

Mühr-Ebert, E.L., Wagner, F., Walther, C., 2019. Speciation of uranium: Compilation of a thermodynamic database and its experimental evaluation using different analytical techniques. Applied Geochemistry 100, 213-222.

Müller, B.R., 2010. Effect of particle size and surface area on the adsorption of albumin-bonded bilirubin on activated carbon. Carbon 48(12), 3607-3615.

Nguyen, T.X., Bhatia, S.K., 2012. Characterization of accessible and inaccessible pores in microporous carbons by a combination of adsorption and small angle neutron scattering. Carbon 50(8), 3045-3054.

Nichols, P., Bylaska, E.J., Schenter, G.K., de Jong, W., 2008. Equatorial and apical solvent shells of the UO22+ ion. The Journal of Chemical Physics 128(12), 124507.

Nolan, P.J., Bone, S.E., Campbell, K.M., Pan, D., Healy, O.M., Stange, M., Bargar, J.R., Weber, K.A., 2021. Uranium(VI) attenuation in a carbonate-bearing oxic alluvial aquifer. Journal of Hazardous Materials 412, 125089.

Nollet, H., Roels, M., Lutgen, P., Van der Meeren, P., Verstraete, W., 2003. Removal of PCBs from wastewater using fly ash. Chemosphere 53(6), 655-665.

Partlan, E., Davis, K., Ren, Y., Apul, O.G., Mefford, O.T., Karanfil, T., Ladner, D.A., 2016. Effect of bead milling on chemical and physical characteristics of activated carbons pulverized to superfine sizes. Water Research 89, 161-170.

Pauletto, P.S., Dotto, G.L., Salau, N.P.G., 2020. Diffusion mechanisms and effect of adsorbent geometry on heavy metal adsorption. Chemical Engineering Research and Design 157, 182-194.

Petrovic, B., Gorbounov, M., Masoudi Soltani, S., 2022. Impact of surface functional groups and their introduction methods on the mechanisms of CO_2 adsorption on porous carbonaceous adsorbents. Carbon Capture Science & Technology 3, 100045.

Philippou, K., Savva, I., Pashalidis, I., 2018. Uranium(VI) binding by pine needles prior and after chemical modification. Journal of Radioanalytical and Nuclear Chemistry 318(3), 2205-2211.

Pourhakkak, P., Taghizadeh, A., Taghizadeh, M., Ghaedi, M., Haghdoust, S., 2021. Chapter 1 - Fundamentals of adsorption technology. In: Ghaedi, M. Interface Science and Technology, Elsevier, 2021, pp. 1-70.

Prajapati, A.K., Mondal, M.K., 2019. Hazardous As(III) removal using nanoporous activated carbon of waste garlic stem as adsorbent: Kinetic and mass transfer mechanisms. Korean Journal of Chemical Engineering 36(11), 1900-1914.

Proriol Serre, I., Vogt, J.-B., Nuns, N., 2019. ToF-SIMS investigation of absorption of lead and bismuth in T91 steel deformed in liquid lead bismuth eutectic. Applied Surface Science 471, 36-42.

Rump, A., Eder, S., Lamkowski, A., Hermann, C., Abend, M., Port, M., 2019. A quantitative comparison of the chemo- and radiotoxicity of uranium at different enrichment grades. Toxicology Letters 313, 159-168.

Saha, D., Grappe, H.A., 2017. 5 - Adsorption properties of activated carbon fibers. In: Chen, J.Y. Activated Carbon Fiber and Textiles, Woodhead Publishing, Oxford, 2017, pp. 143-165.

Sahoo, T.R., Prelot, B., 2020. Chapter 7 - Adsorption processes for the removal of contaminants from wastewater: the perspective role of nanomaterials and nanotechnology. In: Bonelli, B., Freyria, F.S., Rossetti, I., Sethi, R. Nanomaterials for the detection and removal of wastewater pollutants, Elsevier, 2020, pp. 161-222.

Schierz, A., Zänker, H., 2009. Aqueous suspensions of carbon nanotubes: Surface oxidation, colloidal stability and uranium sorption. Environmental Pollution 157(4), 1088-1094.

Schrage, C., Modrow, A., Fichtner, S., Giebelhausen, J.M., Böhringer, B., 2014. Funktionalisierte polymerbasierte sphärische Aktivkohle für Flüssig- und Gasphasenanwendungen. Chemie Ingenieur Technik 86(1-2), 27-34.

Schulte-Herbrüggen, H.M.A., Semião, A.J.C., Chaurand, P., Graham, M.C., 2016. Effect of pH and pressure on uranium removal from drinking water using NF/RO membranes. Environmental Science & Technology 50(11), 5817-5824.

Shang, C., Reiller, P.E., 2020. Determination of formation constants and specific ion interaction coefficients for $Ca_nUO_2(CO_3)_3^{(4-2n)-}$ complexes in NaCl solution by time-resolved laser-induced luminescence spectroscopy. Dalton Transactions 49(2), 466-481.

Shen, J., Schäfer, A., 2014. Removal of fluoride and uranium by nanofiltration and reverse osmosis: A review. Chemosphere 117, 679-691.

Shi, G., Liu, J., Wang, C., Song, B., Tu, Y., Hu, J., Fang, H., 2013. Ion enrichment on the hydrophobic carbon-based surface in aqueous salt solutions due to cation-π interactions. Scientific Reports 3(1), 3436.

Smedley, P.L., Kinniburgh, D.G., 2023. Uranium in natural waters and the environment: Distribution, speciation and impact. Applied Geochemistry 148, 105534.

Song, F., Zhang, Z., Mai, X., Wang, N., Yu, H., Han, Z., Jie, W., Guo, Z., Liu, B., 2021. Efficient removal of U(VI) from aqueous solutions via an activated 3D framework carbon. Journal of Radioanalytical and Nuclear Chemistry 327(2), 721-729.

Speight, J., 2005. Lange's handbook of chemistry, McGraw-Hill Education.

Srivastava, A., Gupta, B., Majumder, A., Gupta, A.K., Nimbhorkar, S.K., 2021. A comprehensive review on the synthesis, performance, modifications, and regeneration of activated carbon for the adsorptive removal of various water pollutants. Journal of Environmental Chemical Engineering 9(5), 106177.

Steen, H., 2004. Geschichte des modernen Bergbaus im Schwarzwald: Eine detaillierte Zusammenstellung der Bergbauaktivitäten von 1890 bis zum Jahr 2000, BoD–Books on Demand GmbH, Norderstedt.

Syed, A.Z., Rienen, U.v., Elter, P., 2013. Effects of Brownian motion on electrical double layer. Biomedical Engineering / Biomedizinische Technik 58(Suppl. 1).

Tagliavini, M., Engel, F., Weidler, P.G., Scherer, T., Schäfer, A.I., 2017. Adsorption of steroid micropollutants on polymer-based spherical activated carbon (PBSAC). Journal of Hazardous Materials 337, 126-137.

Thapa, R., Rahmani, A., Turhanen, P., Taskinen, A., Nissinen, T., Neitola, R., Vepsäläinen, J., Lehto, V.-P., Riikonen, J., 2021. Recovery of uranium with bisphosphonate modified mesoporous silicon. Separation and Purification Technology 272, 118913.

Tian, Y., Liu, L., Ma, F., Zhu, X., Dong, H., Zhang, C., Zhao, F., 2021. Synthesis of phosphorylated hyper-cross-linked polymers and their efficient uranium adsorption in water. Journal of Hazardous Materials 419, 126538.

Torkabad, M.G., Keshtkar, A.R., Safdari, S., 2017. Comparison of polyethersulfone and polyamide nanofiltration membranes for uranium removal from aqueous solution. Progress in Nuclear Energy 94, 93-100.

Tran, H.N., Wang, Y.-F., You, S.-J., Chao, H.-P., 2017a. Insights into the mechanism of cationic dye adsorption on activated charcoal: The importance of π–π interactions. Process Safety and Environmental Protection 107, 168-180.

Tran, H.N., You, S.-J., Chao, H.-P., 2016. Thermodynamic parameters of cadmium adsorption onto orange peel calculated from various methods: A comparison study. Journal of Environmental Chemical Engineering 4(3), 2671-2682.

Tran, H.N., You, S.-J., Hosseini-Bandegharaei, A., Chao, H.-P., 2017b. Mistakes and inconsistencies regarding adsorption of contaminants from aqueous solutions: A critical review. Water Research 120, 88-116.

Tran, T.N., Kim, D.-G., Ko, S.-O., 2018. Adsorption mechanisms of manganese (II) ions onto acid-treated activated carbon. KSCE Journal of Civil Engineering 22(10), 3772-3782.

Trinh, P.B., Schäfer, A.I., 2023. Adsorption of glyphosate and metabolite aminomethylphosphonic acid (AMPA) from water by polymer-based spherical activated carbon (PBSAC). Journal of Hazardous Materials 454, 131211.

Villalobos-Rodríguez, R., Montero-Cabrera, M.E., Esparza-Ponce, H.E., Herrera-Peraza, E.F., Ballinas-Casarrubias, M.L., 2012. Uranium removal from water using cellulose triacetate membranes added with activated carbon. Applied Radiation and Isotopes 70(5), 872-881.

Wang, J., Guo, X., 2020. Adsorption kinetic models: Physical meanings, applications, and solving methods. Journal of Hazardous Materials 390, 122156.

Wang, J., Guo, X., 2022. Rethinking of the intraparticle diffusion adsorption kinetics model: Interpretation, solving methods and applications. Chemosphere 309, 136732.

Wang, X., Cheng, H., Ye, G., Fan, J., Yao, F., Wang, Y., Jiao, Y., Zhu, W., Huang, H., Ye, D., 2022a. Key factors and primary modification methods of activated carbon and their application in adsorption of carbon-based gases: A review. Chemosphere 287, 131995.

Wang, Y., Liu, X., Xie, Y., Chen, B., Zhang, Y., 2022b. Effective and rapid adsorption of uranium via synergy of complexation and cation-π interaction. Journal of Radioanalytical and Nuclear Chemistry 331(2), 1115-1126.

Wang, Z., Bin Kang, S., Won, S.W., 2022c. Polyethylenimine-aminated polyvinyl chloride fiber for adsorption of reactive dyes from single and binary component systems: Adsorption kinetics

and isotherm studies. Colloids and Surfaces A: Physicochemical and Engineering Aspects 647, 128983.

Waseem, A., Ullah, H., Rauf, M.K., Ahmad, I., 2015. Distribution of natural uranium in surface and groundwater resources: A review. Critical Reviews in Environmental Science and Technology 45(22), 2391-2423.

Watts, J.F., Goacher, R.E., 2022. A guide for the meaningful surface analysis of wood by XPS and ToF-SIMS. Surface and Interface Analysis 54(4), 389-404.

WHO, 2017. Guidelines for drinking-water quality: fourth edition incorporating first addendum (https://apps.who.int/iris/rest/bitstreams/1080656/retrieve access date 5/12/2022), World Health Organization, Geneva.

Williamson, A.J., Morris, K., Law, G.T.W., Rizoulis, A., Charnock, J.M., Lloyd, J.R., 2014. Microbial reduction of U(VI) under alkaline conditions: Implications for radioactive waste geodisposal. Environmental Science & Technology 48(22), 13549-13556.

Wolters, J., Tagliavini, M., Schäfer, A.I., 2019. Removal of steroid hormone micropollutants by UF-PBSAC composite in presence of organic matter. Journal of Membrane Science 592, 117315.

Worch, E., 2012. Adsorption technology in water treatment, De Gruyter.

Worch, E., 2021. Adsorption technology in water treatment: Fundamentals, processes, and modeling, De Gruyter, Berlin, Boston.

Wu, Q.-Y., Lan, J.-H., Wang, C.-Z., Xiao, C.-L., Zhao, Y.-L., Wei, Y.-Z., Chai, Z.-F., Shi, W.-Q., 2014. Understanding the bonding nature of uranyl ion and functionalized graphene: A theoretical study. The Journal of Physical Chemistry A 118(11), 2149-2158.

Xie, Y., Chen, C., Ren, X., Wang, X., Wang, H., Wang, X., 2019. Emerging natural and tailored materials for uranium-contaminated water treatment and environmental remediation. Progress in Materials Science 103, 180-234.

Xu, Z., Xing, Y., Ren, A., Ma, D., Li, Y., Hu, S., 2020. Study on adsorption properties of water hyacinth-derived biochar for uranium (VI). Journal of Radioanalytical and Nuclear Chemistry 324(3), 1317-1327.

Yakout, S.M., Abdeltawab, A.A., 2015. Adsorption of uranium in the presence of different ions, humic acid and effect of thorium on uranium adsorption by activated carbon. Desalination and Water Treatment 55(8), 2209-2220.

Yakout, S.M., Metwally, S.S., El-Zakla, T., 2013. Uranium sorption onto activated carbon prepared from rice straw: Competition with humic acids. Applied Surface Science 280, 745-750.

Yaman, M., Demirel, M.H., 2021. Synthesis and characterization of activated carbon from biowaste-peanut shell and application to preconcentration/removal of uranium. Bulletin of Environmental Contamination and Toxicology 106(2), 385-392.

Yang, L., Xiao, H., Qian, Y., Zhao, X., Kong, X.-Y., Liu, P., Xin, W., Fu, L., Jiang, L., Wen, L., 2022. Bioinspired hierarchical porous membrane for efficient uranium extraction from seawater. Nature Sustainability 5(1), 71-80.

Yang, W., Parker, T.G., Sun, Z.-M., 2015. Structural chemistry of uranium phosphonates. Coordination Chemistry Reviews 303, 86-109.

Yi, L., Zuo, L., Wei, C., Fu, H., Qu, X., Zheng, S., Xu, Z., Guo, Y., Li, H., Zhu, D., 2020a. Enhanced adsorption of bisphenol A, tylosin, and tetracycline from aqueous solution to nitrogen-doped multiwall carbon nanotubes via cation-π and π-π electron-donor-acceptor (EDA) interactions. Science of The Total Environment 719, 137389.

Yi, Z., Liu, J., Zeng, R., Liu, X., Long, J., Huang, B., 2020b. Removal of uranium(VI) from aqueous solution by Camellia oleifera shell-based activated carbon: adsorption equilibrium, kinetics, and thermodynamics. Water Science and Technology 82(11), 2592-2602.

Yoshihara, K., Aikawa, M., Machida, M., 2009. Influence of solution pH and background electrolytes on heavy metals ion adsorption by activated carbons from aqueous solutions. Carbon 47(9), 2301.

Yu, F., Ma, J., Han, S., 2014. Adsorption of tetracycline from aqueous solutions onto multi-walled carbon nanotubes with different oxygen contents. Scientific Reports 4(1), 5326.

Yu, X., Zhang, L., Liang, M., Sun, W., 2015. pH-dependent sulfonamides adsorption by carbon nanotubes with different surface oxygen contents. Chemical Engineering Journal 279, 363-371.

Zhang, J., Li, T., Li, X., Liu, Y., Li, N., Wang, Y., Li, X., 2021a. A key role of inner-cation-π interaction in adsorption of Pb(II) on carbon nanotubes: Experimental and DFT studies. Journal of Hazardous Materials 412, 125187.

Zhang, Y., Ye, T., Wang, Y., Zhou, L., Liu, Z., 2021b. Adsorption of uranium(VI) from aqueous solution by phosphorylated luffa rattan activated carbon. Journal of Radioanalytical and Nuclear Chemistry.

Zhao, D., Zhang, Q., Xuan, H., Chen, Y., Zhang, K., Feng, S., Alsaedi, A., Hayat, T., Chen, C., 2017. EDTA functionalized Fe3O4/graphene oxide for efficient removal of U(VI) from aqueous solutions. Journal of Colloid and Interface Science 506, 300-307.

Zhao, J., Lu, P., He, T., Zhang, Q., Huang, J., Liu, Y., Zhao, X., Wang, Y., Liu, Z., Yuan, D., 2023a. Synthesis of core–shell magnetic nanocomposite bearing phosphonic acid ligand for uranium extraction from strong HNO3 solution. Chemical Engineering Journal 468, 143398.

Zhao, J., Yuan, D., Lu, P., Liu, Y., He, Y., Wang, Y., Zhao, X., Liu, Z., Zhang, Q., 2023b. Ultrafast elimination of uranium from aqueous solution by convenient synthesis of phosphonic acid functionalized mesoporous carbon: A combined experimental and density functional theory study. Separation and Purification Technology 315, 123582.

Zhao, W., Liu, D., Feng, Q., 2020. A visualization method for studying the adsorption of lead species in salicylhydroxamic acid flotation of hemimorphite. Minerals Engineering 154, 106434.

Zhu, M., Li, F., Chen, W., Yin, X., Yi, Z., Zhang, S., 2021a. Adsorption of U(VI) from aqueous solution by using KMnO4-modified hazelnut shell activated carbon: characterisation and

artificial neural network modelling. Environmental Science and Pollution Research 28(34), 47354-47366.

Zhu, M., Li, F., Chen, W., Yin, X., Yi, Z., Zhang, S., 2021b. Adsorption of U(VI) from aqueous solution by using KMnO4-modified hazelnut shell activated carbon: characterisation and artificial neural network modelling. Environmental Science and Pollution Research.